Lab on a Chip

Accepted Manuscript

ROYAL SOCIETY OF CHEMISTRY

www.rsc.org/loc

Journal Name

ARTICLE TYPE

Cite this: DOI: 10.1039/xxxxxxxxxx

Active droplet generation in microfluidics

Zhuang Zhi Chong,[a] Say Hwa Tan,*[b] Alfonso M Gañán-Calvo,*[c] Shu Beng Tor,[a] Ngiap Hiang Loh,[a] Nam-Trung Nguyen,*[b]

Received Date
Accepted Date

DOI: 10.1039/xxxxxxxxxx

www.rsc.org/journalname

The reliable generation of micron-sized droplets is an important process for various applications in droplet-based microfluidics. The generated droplets work as a self-contained reaction platform in droplet-based lab-on-a-chip systems. With the maturity of this platform technology, sophisticated and delicate control of the droplet generation process is needed to address the increasingly complex applications. This review presents the state of the art of active droplet generation concepts, which are categorized according to the nature of the induced energy. At the liquid/liquid interface, an energy imbalance leads to instability and droplet breakup.

1 Introduction

In some decades from now, microfluidics could be the key technology for gathering the massive information from chemical and biochemical analysis, diagnosis and therapeutics. However, microfluidics currently cannot match the significance of microelectronics in our every-day life. The early high expectations[1,2] on microfluidics technology have not been met. Table 1 lists the present (as of June 2015) annual growth rate of publications related to microfluidics using different keywords. The current overall growth rate of approximately 2% is significantly lower than the annual 20.5% during the period of 1997-2005. Considering the worldwide growth rate of scientific publications of about 2%, microfluidics research in general may have reached its saturation. Whitesides elaborated some reasons for this trend.[3]

While microfluidic designs in nature are three-dimensional (3D), the majority of microfluidic systems are two-dimensional (2D) due to the use of photolithography[4–7] inherited from microelectronics technology. The current saturation level of publication output may be caused by the 2D limitations for the physics of flows involved such as closed flows, low Reynolds number, strong surface interactions, limited maximum pressures and sensitivity to clogging.

One possible way to create a 3D environment in microfluidics is the intelligent generation of droplets in a 2D microfluidic device, followed by or merged with a more general 3D design.

Table 1 Growth rate of scientific articles (Extracted from Scopus on 8th of June, 2015)

Wording	Annual growth rate (%)
graphene	16.10%
“flow chemistry”	10.64%
microfluidics* & “flow focusing”	4.09%
“flow focusing”	4.08%
microfluidics* & drop*	3.98%
microfluidics* & drop* & control*	3.18%
microfluidics* & T-junction	2.16%
microfluidic*	2.05%
T-junction	1.99%
microfluidics* & *pump*	-0.30%
microfluidics* & valve*	-1.13%
microfluidic* & “drop* form*”	-5.08%
“drop* form*”	-13.16%
(all articles)	2.01%

This merging would generally demand a strict control on the size and time associated to the generated droplet. The formation or generation process of droplets illustrates the complexity of microfluidic handling. The relatively small forces related to interfacial tension makes the droplet formation process highly nonlinear and sensitive to external disturbance. Over the last two decades, droplet formation under a limited set of non-dimensional parameters has been one of the classical hot topics of fluid physics and consequently of microfluidics (Fig. 1).[7–18] The knowledge on the fundamental physics of droplet formation has reached a sufficient level of maturity. Figure 1 indicates that the number of papers with “droplet

[a] School of Mechanical and Aerospace Engineering, Nanyang Technological University, 50 Nanyang Avenue, Singapore 639798.
[b] Queensland Micro- and Nanotechnology Centre, Griffith University, 170 Kessels Road QLD 4111, Brisbane, Australia. Email: sayhwa.tan@griffith.edu.au, nam-trung.nguyen@griffith.edu.au
[c] Depto. de Ingeniería Aeroespacial y Mecánica de Fluidos, Universidad de Sevilla, E-41092 Sevilla, Spain. Email: amgc@us.es

formation" has decreased in favor of a more direct applications of droplet-based microfluidics.

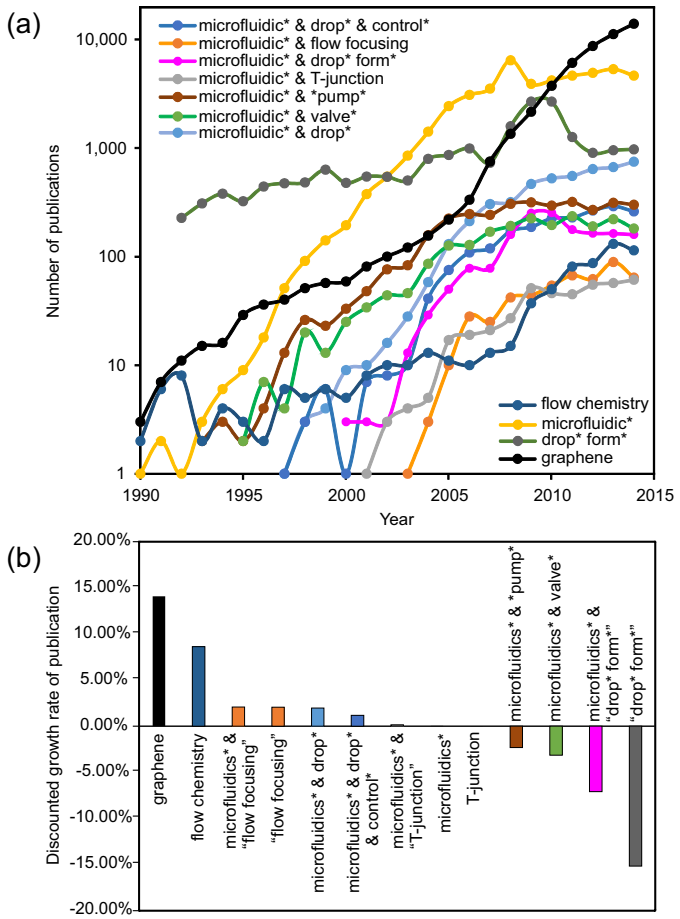

Fig. 1 (a) Evolution of publication number per year using primarily (in title, abstract or keywords) the indicated words. The global publication output is currently about 40 million papers, with an approximately constant growth rate of about 2.5% maintained since 1975. (b) Growth rate of publications per year discounted with the annual growth rate of global publications. (Extracted from Scopus on 8th of June, 2015)

To form a droplet from the continuous liquid phase, energy needs to be introduced to the droplet surface so that a part of the energy is converted into surface energy. That energy may come from hydrodynamic pressure of the flow without any external input, which is known as passive control. Active control is obtained if external energy is locally added to the droplet formation process. Two most widely used configurations for passive droplet formation are the T-junction[6,12,19] and the flow focusing junction.[7,20–24] The flow focusing junction can be further categorized as cross-junction (planar[25,26] or axisymmetric[22,27]) and genuine flow focusing. Genuine flow focusing discharges the droplets into an open environment, or a significantly wider channel.[7,20,28] Historically, the first flow focusing configuration proposed was symmetric,[20,29] even though the original patent[30] covered both axisymmetric and planar configurations. Stone's group[7] performed a simple but remarkably successful translation of this concept into the planar microdevice.

In both configurations, droplet formation can be controlled passively by varying the flow rate or the applied pressure.[31] Syringe pumps are usually employed to drive the flow with a controllable flow rate, while a gravity based pressure unit or a pressure controller are used for pressure driven flows. The major drawback of passive control is the slow response time in the order of seconds or even minutes.[32] The long response time comes from the relatively large fluidic resistance of the tubing and the fluidic capacitance caused by the compressibility of the liquid or the channel material.[33,34] The only way to achieve a specific droplet size with preset flow rates or pressures is by adjusting the liquid properties and channel geometries.

A significant number of review papers on droplet-based microfluidics exists in the literature. These previous reviews discussed the device fabrication,[35] production and/or manipulation of droplets,[35–42] fusion or fission.[35,37–40] To our best knowledge, no review paper dedicated exclusively to the active control of droplet generation. A book chapter briefly discussed the active control of droplet formation,[43] it was limited to thermal and magnetic control only. Christopher et al.[36] devoted a section discussing the active control methods using pneumatic/hydraulic valves, piezoelectric actuation and electric field. Teh et al.[37] briefly mentioned pneumatic valve and electrowetting in their review. Baroud's review[38] has a small section on control using laser, pneumatic/hydraulic valve and heater. Seemann et al.[35] discussed "active elements" in droplet generation devices such as pneumatic/hydraulic valves, heaters, and piezoelectric actuators. Chen's review paper[40] mentioned pneumatic pressure, optical, and electric methods. Song et al.[41] discussed thermal control and chopper method in their review. Theberge et al.[39] and Zhao et al.[42] just listed active methods such as electrical, mechanical and thermal approaches in their review.

In the present review, we will focus specifically on closed-channel microfluidic systems.[11] The length scales of the characteristic flow channels are smaller than one millimeter.[33] We only consider the flow of two phases. The liquid of the droplets is the dispersed phase, and the surrounding liquid is the continuous phase. The review discusses (i) active control methods according to the type of external energy for activation, (ii) the fundamental mechanism to introduce such energy, (iii) the typical implementations of each method, (iv) the comparison among alternative methods in terms of efficiency, speed, compactness, robustness and reproducibility, and (v) the perspectives on their improvements. While 3D or open microfluidic designs use a wide variety of active methods (often inherited from other fields), those cannot be immediately imported, or not applicable at all in closed channel microfluidics.

2 Electrical control

Electric energy can be used to manipulate droplet generation. The combination of both mechanical and electric focusing forces at the microscale was initially proposed in a 3D configuration.[49,50] That concept was subsequently incorporated in a 2D or planar microfluidic configuration by Anna et al.[7] and Link et al.,[44] following the same path as the original 3D flow

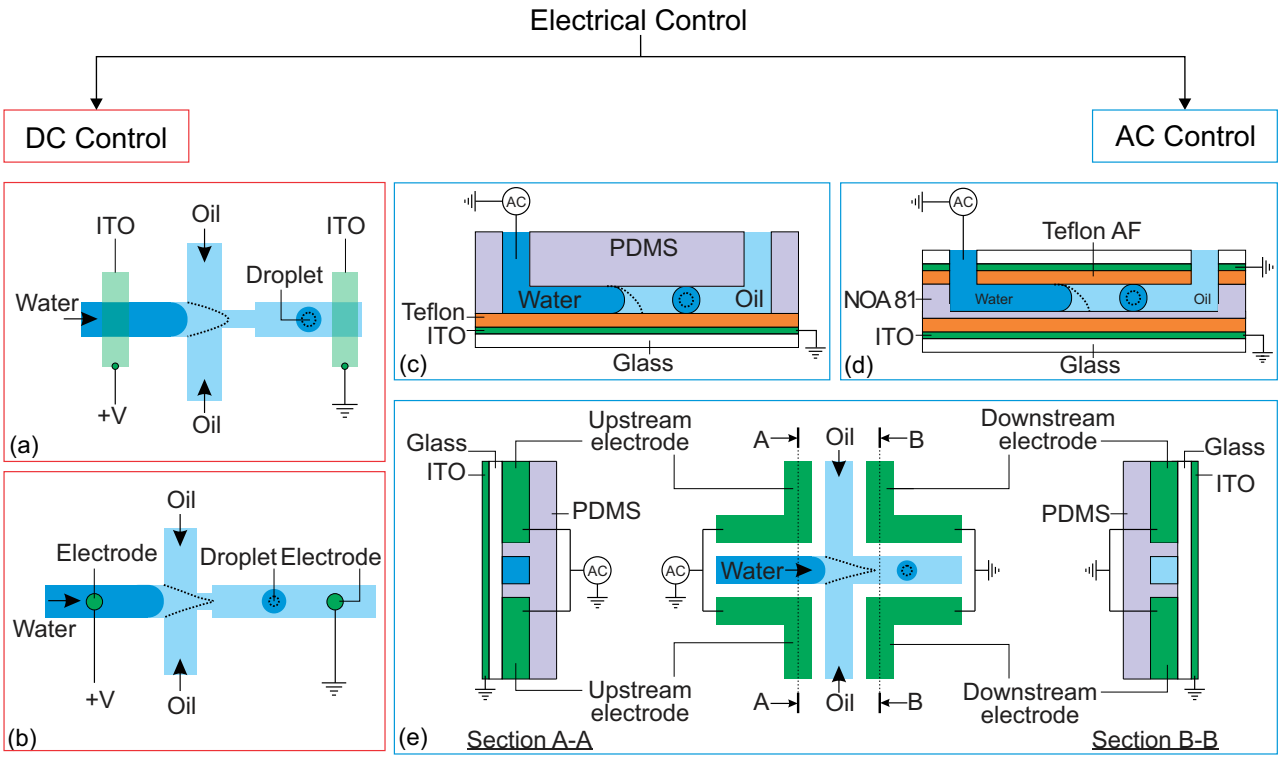

Fig. 2 Classification of electrical control approaches (a) Application of direct current on flow focusing configuration. The indium tin oxide (ITO) are patterned on a glass slide before being bonded with a PDMS device[44] (b) Flow focusing configuration with electrodes contacting the fluids via insertion through PDMS[45] (c) Flow focusing device with EWOD control.[46] (d) Flow focusing device fabricated using NOA 81 with EWOD control. An extra ITO electrode is placed on top of the channel to increase the effect of EWOD[47] (e) Flow focusing device fabricated with electrodes and its electrical connections. The dotted lines illustrate the changes after activation of the electrical control.[25,48]

focusing.[20,51] Combining forces of a completely different origins requires special consideration for the geometry and location of the electrodes. The electrodes should provide a main electric field component not only aligned with the mechanical force, but also having its maximum located around the same (focusing) region of the force.[52] The electrodes integrated in the system could either be in contact with the liquids or separated by a dielectric material to prevent electrode fouling.

Electrical control of droplet generation can be categorized according to the type of the current applied to the electrodes, Fig. 2. For direct current (DC) control, the magnitude of voltage remains constant throughout the application of the current. For alternating current (AC) control, the voltage fluctuates with a frequency that is different than that of the droplet generation. For high-frequency AC control, the frequency of the control signal is much higher than that of droplet generation. Therefore, the droplet generation frequency forms the characteristic time of the system.

2.1 Direct current

Link et al.[44] employed a DC voltage to control the droplet formation in a microfluidic setup, Fig. 2(a). The planar flow focusing device had two electrodes made of indium tin oxide (ITO). The ITO electrodes were patterned on top of a glass slide before being bonded[53] to the PDMS part with microchannels. These electrodes had a direct contact with the liquids inside the channel. With an appropriate electrode design, the process of droplet formation changes upon application of a high voltage to a relatively conducting (or leaky dielectric[54]) liquid stream, Fig. 2(a). Water as a paradigmatic leaky dielectric has been extensively used in microfluidics. Water allows its free charges to quickly migrate in opposite directions under the applied electric field, until they hit the water-oil interface, where they accumulate.[55]

Under a fixed set of flow rates, droplet size decreases with increasing applied voltage, as result of charge accumulation at the interfaces. The droplet volume can decrease by three orders of magnitude by increasing the voltage alone. In tangible terms, increasing the applied electric field $E \sim V/d$ demands an increase of interfacial area per unit volume $1/d$ to accommodate the extra induced charges, where V is the applied voltage and $1/d$ is the characteristic surface curvature or the inverse of droplet size. This phenomenon can also be understood in terms of a simple capacitor model. The droplet interface between the conductive water stream and the isolating oil stream acts as a capacitor, where the surface charge $q \sim \varepsilon_0 E$ increases with the applied voltage. A larger surface area per unit volume, or overall surface curvature, leads to an increase in surface energy associated to surface tension. The normal stress balance at the water-oil interface is

$$\gamma C = p + \{\varepsilon_0 E_{0,n}^2 + (\varepsilon_i - \varepsilon_0) E_{i,n}^2 - \varepsilon_i E_s^2\} \quad (1)$$

where γ, ε_0, ε_i, $E_{0,n}$, $E_{i,n}$ and E_s are the water-oil interfacial

tension, electric permittivities of water and oil, the normal components of the outer (oil) and inner (water) electric fields, and the tangential component of the electric field, respectively. And C is the local curvature of the interface. As long as the corresponding local increment in electric forces can be balanced by surface tension, the system remains balanced and stable. The local hydrostatic pressure p in the flow acts as a *reservoir* to guarantee the total surface stress balance at the water-oil interface as long as the electric stresses do not overcome the surface tension:

$$\frac{\gamma}{d} \gtrsim \varepsilon_0 E^2 \sim \varepsilon_0 \left(\frac{V}{d}\right)^2 \quad (2)$$

However, as V increases, the electric forces grow faster (roughly as d^{-2}) than the surface tension (as d^{-1}) leading to instability, surface disruption, and the ejection of droplets. In other words, instability sets in when the local symmetry (balance) provided by equation (1) is no longer possible. The increasing electric force decreases the break up time $t_c \sim (\frac{\rho d^3}{\gamma})^{1/2}$, thus forming smaller droplets under constant flow rates. If the applied voltage is too large, the interface anchored at the outlet and the issuing droplet becomes highly charged at pinch off. The charge causes both of them to repel against each other, promoting the droplet formation instability.

Electric control with direct current does not require moving parts. Besides, as charging and discharging of the interface can be quickly performed, the response time is reduced down to 10 μs.[44] However, electrode fouling is the main drawback of this technique. The upstream electrode is constantly in contact with the dispersed phase, while the downstream electrode only makes contact as the highly charged water droplets pass by. The electrode in contact with water is susceptible to fouling and could affect the reliability of the system.[56] Furthermore, the droplets produced by this approach are charged, and may not be suitable for sensitive chemical or biological samples.

The above concept was continued by Kim et al. without the ITO electrode.[45] The electrodes contact the fluids through a metal wire directly inserted through the PDMS. Figure 2(b) shows this setup. Similar to Link's result, the droplet size decreases with an increasing applied voltage. However, instead of becoming an unstable stream when the applied voltage is too large, the dispersed stream of this setup forms a jet connecting the stream source to the ground electrode located downstream. Fine droplets with diameter less than 1 μm were formed at a relatively low flow rate ratio between the dispersed the continuous phase. The droplets are claimed to be formed from the tip of a Taylor cone, a cone-shape interface with 49.3° half-angle apex balanced by electrostatic force and surface tension.[57] However, the Taylor cone formed under this setup could only be kept stable for about a minute due to the pulsation exerted by the syringe pump run at a low flow rate.

2.2 Alternating current

In contrast to DC control, the electrodes of this approach are connected to an alternating current (AC) voltage. In terms of frequency, electric control with AC voltage can be further categorized into the two groups of low-frequency and high-frequency control. Frequency lower than the frequency of droplet generation is considered as low. Frequency above the droplet generation frequency is considered high. At low-frequency control, droplet generation is asynchronous and out of phase with the applied AC voltage, causing differences in the charge of individual droplets. The low-frequency approach was attempted by Kim to improve the repeatability of Taylor cone formation.[45] A pulse of 200 ms, with about 25 ms to ramp up/down and an amplitude between 0 and 2000 V was applied to the electrodes. The Taylor cone is formed once per pulse.

Later, He et al. used a setup similar to Kim's to investigate the response of droplet formation under low-frequency AC control.[58] In this work, the triangular AC signal had a frequency of 10 Hz and an amplitude of 2 kV. Interestingly, the change in the droplet size was independent of the polarity of the voltage. However, that change exhibited a hysteresis effect with the applied voltage. The droplet size decreased rapidly during the initial stage of the voltage ramp up. The droplet size then reached its minimum at about the middle of the ramp-up stage, before increasing slowly for the second half of the ramp-up stage. The droplet size continued to increase gradually for the whole ramp-down stage before restoring the original size near the end of the ramp-down stage. This phenomenon is related to the relaxation of the flow rate oscillation, which can be explained by a model analogous to an RC electric circuit with varying resistance.[58]

In high-frequency control, the average applied voltage during the generation of each droplet is approximately zero. In this approach, the droplet size is tuned by the frequency and the root-mran-square amplitude of the AC voltage. Electrowetting phenomenon can be observed in an electrolyte droplet on top of an electrode. The contact angle decreases upon application of a voltage across the electrolyte and the electrode. However, this phenomenon is typically only applicable up to about a hundred millivolts, before the occurrence of electrolysis.[59] The electrolysis problem is addressed by having a thin insulating film between the electrode and the electrolyte.[60] This configuration, also known as electrowetting on dielectric (EWOD), allows the application of a large voltage that reduces the contact angle further. Although both DC and AC can be used for EWOD, AC is generally superior as it reduces the contact angle hysteresis.[61] To our best knowledge, manipulation of droplet generation based on EWOD has been reported with AC voltage only. Maloggi et al. introduced the use of EWOD to control droplet generation on a flow focusing device.[46] The device consists of a PDMS part with flow focusing channels attached to an ITO glass pre-coated with a ~4-μm thick Teflon film, Fig. 2(c). An AC voltage (10 kHz, 0-170 V_{rms}) was applied on the aqueous phase through a thin wire while the ITO is grounded. NaCl solution served to enhance the conductivity of the aqueous phase. Both liquid phases were delivered individually into the device using hydrostatic heads.

The effect of electrowetting on the oil-water interface is indicated through the critical external water pressure P_W^* required to sustain the interface at the flow focusing junction at a given external oil pressure P_0. The water pressure P_W^*

decreases with increasing voltage V_{rms}:

$$P_W^*(V_{rms}, P_0) = P_L(V_{rms}) + \lambda P_0, \quad (3)$$

where $P_L(V_{rms})$ is the maximum Laplace hydrostatic pressure to sustain the oil-water interface, λ is a constant that depends on the hydrodynamic resistances of the channels. This model assumes that P_W^* needs to exceed the sum of $P_L(U)$ and λP_0 before droplets are generated.

In equation (1), the local surface curvature is expressed as $C = (\frac{1}{R_w} + \frac{1}{R_h})$, where R_w and R_h are the two radii of curvature of the surface. In an analogous way as with DC control, when an AC voltage is applied to the aqueous phase, the contact angle on the Teflon film decreases and R_h increases. In addition, increasing voltage V_{rms} may lead to an increasing electric stress on the oil-water interface. Both effects force a decrease of water pressure P_W^* to maintain the balance equation (3). With constant R_w and γ, $P_L(V_{rms})$ decreases under the applied AC voltage. This model explains well the decrease of P_W^* with increasing V_{rms} in the experiment. Under a constant set of pressures, the droplet size increases with increasing voltage.[62] This effect is similar to an increase in the water flow rate owing to a smaller hydrostatic pressure at the outlet of the water channel. Since the shear viscous forces dominate in the oil flow, the ratio between the viscous force and the electrostatic force on the water surface grows,[62] causing its destabilization. Mallogi et al. also reported on-demand generation of droplet using the same setup by applying AC pulses. Droplet starts to form above a critical pulse width. The droplet volume could be tuned by the pulse width.

Active control using EWOD does not need a counter-electrode in contact with the fluids flowing at the downstream channel. Furthermore, the applied voltage is much smaller than that needed for DC control. The lower voltage is more gentle for the electrode contacting the aqueous stream. However, the effectiveness of EWOD reduces dramatically if the interfacial tension is reduced by addition of the surfactants such as Span 80 and Triton X-100.[62]

Gu et al.[63] reported a similar approach but using a much smaller orifice.[64] Instead of driving the oil flow using hydrostatic pressure, a syringe pump was used. A regime called tip-streaming was observed at low water pressure. The droplets formed in this regime had diameters between 1-2 μm and had a high spatial density. This phenomenon is similar to that caused by surfactant accumulation near the meniscus tip, as described by Anna and Mayer.[65] Gu et al. used a master parametric map[64] to show that upon increasing the applied voltage over a critical value from this regime, a "conical spray" regime occurred. In this regime, the droplets repel each other and spread out upon exiting the orifice. Interestingly, in this regime, the average droplet size increases with increasing voltage. The observed phenomenon might be related to the interplay between the extremely short relaxation timescale of surfactant molecules at the interface tip and the applied frequency. However, in the dripping regime, the droplet size decreases with increasing voltage, as predicted by the equation (1).

In terms of device material, Gu et al. made the EWOD device of Norland Optical Adhesive (NOA).[47] This material has a higher stiffness than PDMS, which enables the fabrication of channels with dimensions down to a few micrometers with a small aspect ratio. Furthermore, the material is compatible with a wider range of oils as compared to PDMS. Fig. 2(d) shows that the effectiveness of electrowetting is further increased by having two ITO electrodes located on the top and the bottom of the microchannel. Before using the device, the microchannels underwent salinization treatment to make them hydrophobic and more sensitive in electrowetting control. In this setup, both oil and water flow rates are driven by syringe pumps. Compared to PDMS devices, EWOD control on NOA devices is more stable. As two electrodes are located on the top and the bottom of the channel, the droplet size is more sensitive to the change in voltage.

EWOD based control requires one of the electrodes to contact with the aqueous liquid. Thus, the electrode is still susceptible to fouling. The response of EWOD to AC voltage starts to deteriorate upon reaching a critical frequency at around 1 kHz for DI water with low conductivity.[66] Lower AC frequency may limit the production rate of monodispersed droplets. To address this problem, Tan et al. suggested a design different than the typical EWOD setup, where all the electrodes are not in contact with the liquids.[25,48] This approach allows a higher frequency up to 50 kHz to control the generation of low conductivity DI water droplets. Fig. 2(e) illustrates the design of the planar flow focusing device. Four electrodes, two upstream and two downstream, around the junction of the flow channel. The device is bonded to an ITO-coated glass. The ITO side is facing outward and does not contact the microfluidic channels. The electrodes were made by filling the microfluidic channels with indium using the technique called microsolidics.[67] The live terminal of the AC power supply is connected to the upstream electrode pair while the downstream electrode pair and the ITO film were grounded.

Under a constant set of flow rates, the droplet formation regime changes upon application of the AC voltage. Generally, the droplet size decreases with increasing voltage. The droplet generation process also depends on the frequency and the conductivity of the aqueous phase. The initially dripping regime changes to the jetting regime when high enough AC frequency is applied while using aqueous phase with low enough conductivity. Dripping regime remains unchanged at low AC frequency and high conductivity. Interestingly, the droplet formation is unstable at the intermediate range of AC frequency and conductivity.

Experimental results suggest that the droplet size at the dripping regime was related to the voltage difference between the oil-water interface and the downstream electrodes. However, as the electrodes are not in contact with the liquids and measuring the voltage at the interface is difficult, the RMS voltage at the tip (U_{tip}) of the interface can be deduced using an RC circuit model. From that model, one obtains the equation,

$$U_{tip} = U_{app}\left(1 + \frac{1}{C_E/C_I + 2\pi j(f/\kappa)(C_E/l)}\right)^{-1}, \quad (4)$$

Table 2 Electrical control

Source	Type of current	Flow channel geometry[1]	Fluids[2]	Notes
44	Direct current	Flow focusing: Orifice $W = 30$	C = oil D = water	Voltage $\leq$ 800 V * Channel H is not stated
45	Direct current, low-frequency pulse current	Flow focusing: H = 61.4, W = 100 Orifice W = 50 Downstream W = 150	C = mineral oil + 6% Span 80 D = distilled water	Voltage $\leq$ 2000 V Pulse frequency = 5 Hz
58	Low-frequency ac	Flow focusing: H = 50, W = 92.7, 83.6 Orifice W = 46.3 Downstream W = 140	C = mineral oil (30 cP) + 6% Span 80 D = distilled water	Triangular ac voltage from -2 to 2 kV, 10 Hz
46	High-frequency ac	Flow focusing: H = 55, 115, 160, 190 W=390	C = mineral oil (30 mPa.s) D = DI water + NaCl (1 S.m^{-1})	10 kHz AC source Voltage $\leq$ 170 V_{rms}
62	High-frequency ac	Flow focusing: H = 100, W = 390	C = mineral oil (30 mPa.s) D = DI water + NaCl (1 S.m^{-1}) For experiments with surfactants, either D + 0.1% Triton X-100 or C + 0.1% Span 80	10 kHz AC source Voltage $\leq$ 150 V_{rms}
63	High-frequency ac	Flow focusing: H = 50, W = 100 Orifice W = 50	C = mineral oil + 3% Span 80 D = DI water + NaCl (0.5 S.m^{-1})	10 kHz AC source Voltage $\leq$ 55 V_{rms}
64	High-frequency ac	Flow focusing: H = 50, W = 200 Orifice W = 50	C = mineral oil (30 mPa.s) + 5% Span 80 D = DI water + NaCl (0.5-0.7 S.m^{-1})	10 kHz AC source Voltage $\leq$ 70 V_{rms}
47	High-frequency ac	Flow focusing: H = 10, W = 100 Orifice W = 20	C = mineral oil (30 mPa.s) + 5% Span 80 D = DI water + NaCl (0.5-0.7 S.m^{-1})	10 kHz AC source Voltage $\leq$ 100 V_{rms}
25,68	High-frequency ac	Flow focusing: H = 35, W = 100	C = mineral oil (30 mPa.s) + 5% Span 80 D = DI water + NaCl (3×10^{-5}-0.3 S.m^{-1})	5-50 kHz AC source Voltage $\leq$ 1000 V_{rms}

[1] H - height in μm; W - width in μm [2] C - continuous phase; D - dispersed phase

where U_{app} is the RMS voltage applied at the upstream pair electrodes, C_E is the capacitance between the electrodes and the aqueous phase, C_I is the capacitance between ITO and the aqueous phase, $j^2 = -1$, f is the AC frequency, κ is the conductivity of the aqueous phase, and l is a geometrical constant. The results converge closely to a single curve on the graph of droplet diameter against U_{tip}.

Apart from the electrical model, Tan et al.[25] also proposed an electrohydrodynamic model that takes Maxwell stresses into consideration. The model relates the droplet size to an effective capillary number, Ca_{eff}:

$$Ca_{eff} = \frac{Ca}{1 - B_e}, \quad (5)$$

where Ca is the classical capillary number and B_e is the electric Bond number comparing the Laplace pressure with the Maxwell stress.[66] Although this model is able to describe the droplet generation process at high frequency, it does not account for the conductivities of the fluid. Tan et al. later used this system to demonstrate the ability to swiftly modulate the frequency of the droplet generation with a response time down to a few milliseconds.[68] By modulating the frequency in the range of 170-340 Hz, the system is fast enough to represent the main music tune of *Ode to Joy* in real time. The music tune is 'played' from the fluorescence signal tracing the frequency of the droplet generation. The system is also able to represent the more challenging main music tune of the *Flight of the Bumblebee* with faster and larger frequency switching and larger error in the target frequency.

3 Thermal control

Thermal control of droplet generation can be categorized into two approaches according to the way the heat is introduce. The first approach utilizes resistive heating at the junction where the droplets are formed. The temperature is controlled by the applied current and feedback from a temperature sensor. The second approach utilizes a focused laser beam to achieve localized heating. Fig. 3 gives an overview on both approaches. Each approach has its own merits and limitations which are discussed as follow.

The use of resistive heating to manipulate droplet size was first introduced by Nguyen's group.[69,73] An integrated microheater and temperature sensor were used to control both the droplet generation regimes and the droplet size in a microfluidic flow-focusing configuration, Fig. 3(a).[69] Microheater and temperature sensor made of platinum were fabricated using a standard lift-off process. The heater and sensor were insulated from the fluids by a thin PDMS layer to avoid charging of the fluids or possible electrolysis.

Thermal control is based on the temperature dependency of the fluid properties, mainly the viscosity and interfacial tension. For most fluids, viscosity and interfacial tension decrease with increasing temperature. This change is reflected in the change in capillary number Ca. In passive droplet generation, the capillary number is often used to characterize both the diameter and formation regime of the droplets. The dependency of the normalized droplet diameters for the set of fluids used was

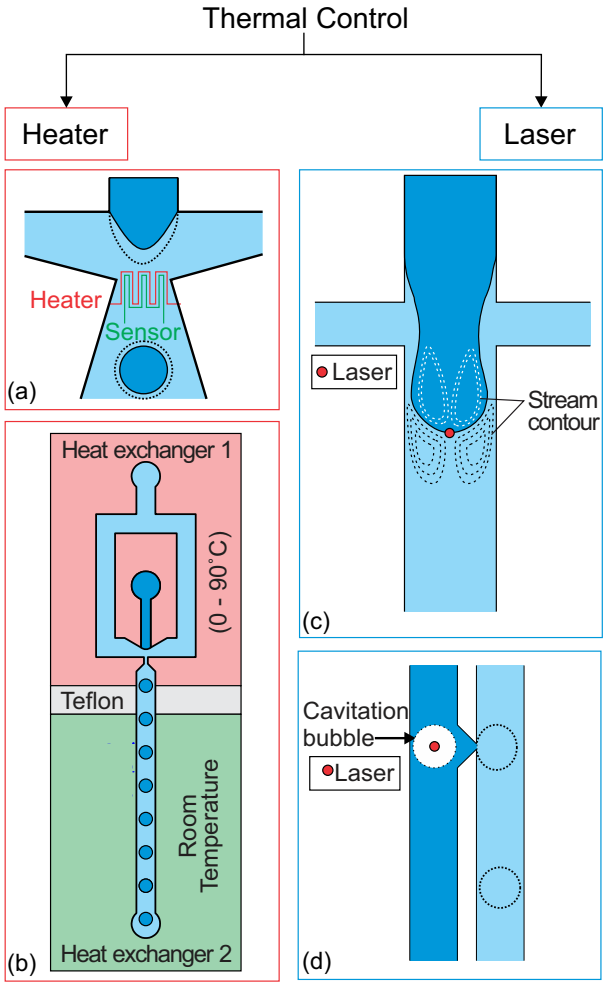

Fig. 3 Two approaches for thermal control (a) Flow focusing geometry with integrated heater and temperature sensor at the orifice of the droplet formation.[69] (b) Heat exchanger regulates the temperature of the upstream part at a temperature ranging from 0 to 90°C. The other one keeps the downstream channel at room temperature. Teflon separates the heat exchangers as an insulator.[70] (c) Location of the spot applied with localized heat by laser and the stream contour of the Marangoni flow formed around the droplet.[71] (d) Droplet on demand produced by creating cavitation bubbles using high intensity laser. The dotted lines illustrate the changes after activation of the thermal control.[72]

expressed as[69]

$$D^*(\Delta T) \propto \frac{\gamma^*(\Delta T)}{\eta^*(\Delta T)} = e^{0.02\Delta T}, \quad (6)$$

where D^*, γ^* and η^* are the diameter, interfacial tension and viscosity normalized by values at a reference temperature. The diameters of the droplets increase by about 2 times with temperature increasing from 25°C to 70°C. The above exponential scaling is only valid for the given fluid system, and does not fully describe the complex nature of thermal control of droplet generation. Factors such as Marangoni effect due to the spatial temperature distribution, surfactant concentration, flow rate ratios, accuracies in both viscosity and surface tension measurements and droplet formation regimes were neglected and not considered in the analysis. This approach offers the compactness and portability required by different lab on a chip applications due to the small footprint. However, the fabrication of the micro-heater and temperature sensor is complicated. The alignment of the microheater and temperature sensor at the desired location adds further complexity towards the implementation of this concept.

The same group extended the work further to investigate the effect of nanoparticles in different microfluidic geometries and channel heights.[74–76] Spherical TiO_2 nanoparticles of 15-nm diameter were added to water leading to a reduction of the interfacial tension between water and oil. The reduction was attributed to the Brownian motions of the nanoparticles. Viscosity and interfacial tension decrease almost linearly with increasing temperature.[74] A microfluidic T-junction device with channel height of about 90 μm, side channel width of 50 μm and main channel width of 150 μm was used to investigate the temperature dependence of the droplets formed using both DI water and DI water with nanoparticles as the dispersed phase fluids. Experimental results showed that for the case of DI water, the size of the droplet increases slightly from about 180 to 190 μm. However, with the nanoparticles, the size of the droplet increases from about 220 to 260 μm. The small sensitivity to temperature is caused by the squeezing regime of droplet formation.[12] The capillary number Ca are 2.8×10^{-3} and 4.1×10^{-3}. With these small Ca numbers, pressure forces dominate over the viscous forces and the size of the droplets depends mainly on the applied flow rate ratio. Therefore, the size of the droplets correlates weakly with the temperature. However, if the channel height is reduced from 90 to 30 μm, the temperature dependence of the droplet size increased due to the larger temperature gradient.[75] Interestingly, the temperature dependence of nanofluid droplets changes when a flow focusing configuration was used.[76] In this configuration, both DI water and nanofluid exhibit similar characteristics in droplet formation at different temperatures. However, the transition between the droplet formation regimes differs for both fluids. This difference is caused by the complex behavior of nanofluids, which introduces factors such as interfacial slip and Brownian motions.

Heating the entire microfluidic device also provides thermal control. Stan et. al.[70] placed a microfluidic flow focusing droplet generator on a pair of heat exchangers. One heat exchanger regulates the temperature of the upstream part from 0 to 90°C, while the other exchanger keeps the downstream channel at room temperature, Fig. 3(b). Three continuous liquid phases were Light mineral oil (Sigma Aldirch 330779), Dynalene SF and Perfluoroperhydrophenanthrene (PFP, Alfa Aesar L17370). Dyanalene SF showed the largest increase in water droplet size. At 70°C, the droplet volume is 100 times smaller the original volume at 10°C. The use of the heat exchanger extended the range of temperature below room temperature and avoided the integration of micrometer and temperature sensors.

Localized heating at the droplet generation site can be achieved precisely with a focused laser beam. Heating using laser is more flexible as the position of the focused laser spot can be adjusted easily. Baroud et al. used a focused laser beam to achieve active control of droplet generation.[71] An argon-ion

Table 3 Thermal control

Source	Heating element	Flow channel geometry[1]	Fluids[1]	Notes[1]
69	Platinum microheater	Flow focusing: H = 70 Orifice W = 45 Channel W = 200	C = MO + 2%$_{w/w}$ Span 80 D = DI water + 0.05%$_{w/w}$ FD	T = 25 - 75 Q_C=600, Q_D=50: +∼200% from d=39.6 Q_C=800, Q_D=100: +∼180% from d=30.9
74	Platinum microheater	T-junction: H = 90 Main W = 150 Side W = 50	C = MO + 2%$_{w/w}$ Span 80 D_1 = DI water + 0.1%$_{vol}$ spherical TiO_2 + 0.05%$_{w/w}$ FD D_2 = DI water + 0.05%$_{w/w}$ FD	T = 25 - 56 Q_C=300, Q_D=60: +5.6% from d=180 with D_1 +16.1% from d=224 with D_2
76	Platinum microheater	Flow focusing: H = 30 Orifice W = 45 Channel W = 200	C = MO + 2%$_{w/w}$ Span 80 D_1 = DI water + 0.1%$_{vol}$ spherical TiO_2 + 0.05%$_{w/w}$ FD D_2 = DI water + 0.05%$_{w/w}$ FD	T = 25 - 45 Q_C=60, Q_D=5: +97% from d=61.8 with D_1 +153% from d=49.3 with D_2
75	Platinum microheater	T-junction: H = 300 & 30 Main W = 100 Side W = 50	C = MO + 2%$_{w/w}$ Span 80 D_1 = DI water + 0.05%$_{w/w}$ FD D_2 = DI water + 0.1%$_{vol}$ spherical TiO_2 + 0.05%$_{w/w}$ FD D_3 = DI water + 0.1%$_{vol}$ cylindrical TiO_2 + 0.05%$_{w/w}$ FD	T = 25 - 39 H=300, Q_C=120,Q_D=60: +12% from d=334 with D_1 H=30, Q_C=12,Q_D=6: +53% from d=85 with D_1 +12% from d=68 with D_2 -15% from d=106 with D_3
70	Heat exchanger	Flow focusing: H = 125 Orifice W = 40 Channel W = 200	C = Dynalene SF D = Water	T = 10 - 70 Total flow rate = 5.3 mL/h Volume increases 100 times of the original volume
71	Argon-ion laser	Cross junction: H = 30 Side W = 125 Main W = 200	C = hexadecane + 2%$_{w/w}$ Span 80 D = Water + 0.1%$_{w/w}$ fluorescein	Laser power = 80 mW Q_C=54,Q_D=4.8: Droplet volume increases about 2 times than the original volume
72	Q-switched Nd:YVO_4 pulsed laser	Parallel channels with orifice: H = 100, W = 100	C = Corn oil D = Phosphate-buffered saline buffer	Q_C=200-6,500, Q_D=12,000-190,000: Droplet on demand generation with frequency up to 10,000

[1] C - continuous phase; D - dispersed phase; MO - mineral oil (Sigma M5904); FD - fluorescence dye (Sigma F6377);
H - height in μm; W - width in μm; d - diameter in μm; T - temperature in °C;
Q_C - continuous phase flow rate in μL/h; Q_D - dispersed phase flow rate in μL/h;
spherical TiO_2 has size of 15 nm; cylindrical TiO_2 has size of 10×40 nm

laser with a wavelength of 514 nm was focused slightly downstream of a cross junction, Fig. 3(c). During the droplet generation process, the advancing oil-water interface was blocked at the laser spot (80 mW beam power, 5.2 μm beam waist). The interface continues to advance downstream as the viscous stress grows to overcome the blocking force. As the droplet formation process is delayed under constant flow rates, the droplet size is about 2 times bigger than that produced without heating with laser.

Tracing microparticles indicated that a flow is generated around the laser spot. The dashed lines in Fig. 3(c) represents the flow pattern schematically. This flow was induced by induced by Marangoni effect. Localized heating led to a large temperature gradient and consequently a surface tension gradient at the liquid interface.[71] The induced flow is large enough to prevent the interface from advancing downstream. The blocking time is directly proportional to the beam power. For instance with a continuous phase flow rate of Q_c=6 μL/h and a dispersed phase flow rate of Q_d=0.18 μL/h, the blocking time increases from 0.8 to 1.6 s with laser power increasing from 60 to 80 mW. The focused laser beam has also been applied to merge two droplets, to fuse droplets at formation, to split droplets, and to direct the droplets.[77]

Extending the concept of laser heating, Park et al. applied a pulse laser on a stable water-oil interface[72] to generate water droplets on demand with a valve, Fig. 3(d). The laser beam caused localized heating with boiling and rapidly created a cavitation bubble. The bubble injects a droplet from the interface into the surrounding oil phase. The flow rates used in that work ranged from 12 to 190 mL/h for water and 0.2 to 6.5 mL/h for oil. A laser with high pulse frequency would allow a high droplet generation rate up to 10,000 droplets per second. However, as the process is temperature dependent and repeated laser pulses steadily increase the temperature of the system, the system temperature has to be regulated.

4 Magnetic control

A liquid may exhibit a bulk dynamic response to a magnetic field. Magnetism allows contactless actuation in microfluidics such as pumping, mixing, trapping, separation and detection.[82,83] Magnetism has also been adopted to control the generation,[19] transport,[84,85] splitting,[86] morphology manipulation[87] and positioning[88] of droplets. Here, we focus only on droplet generation. Magnetic fluids such as ferrofluids are liquids with suspended magnetic particles. Magnetic fluid may serve as either the dispersed phase or the continuous phase.[89] The interparticle magnetic energy in a ferrofluid is weak because of the small particle size of less than 10 nm and

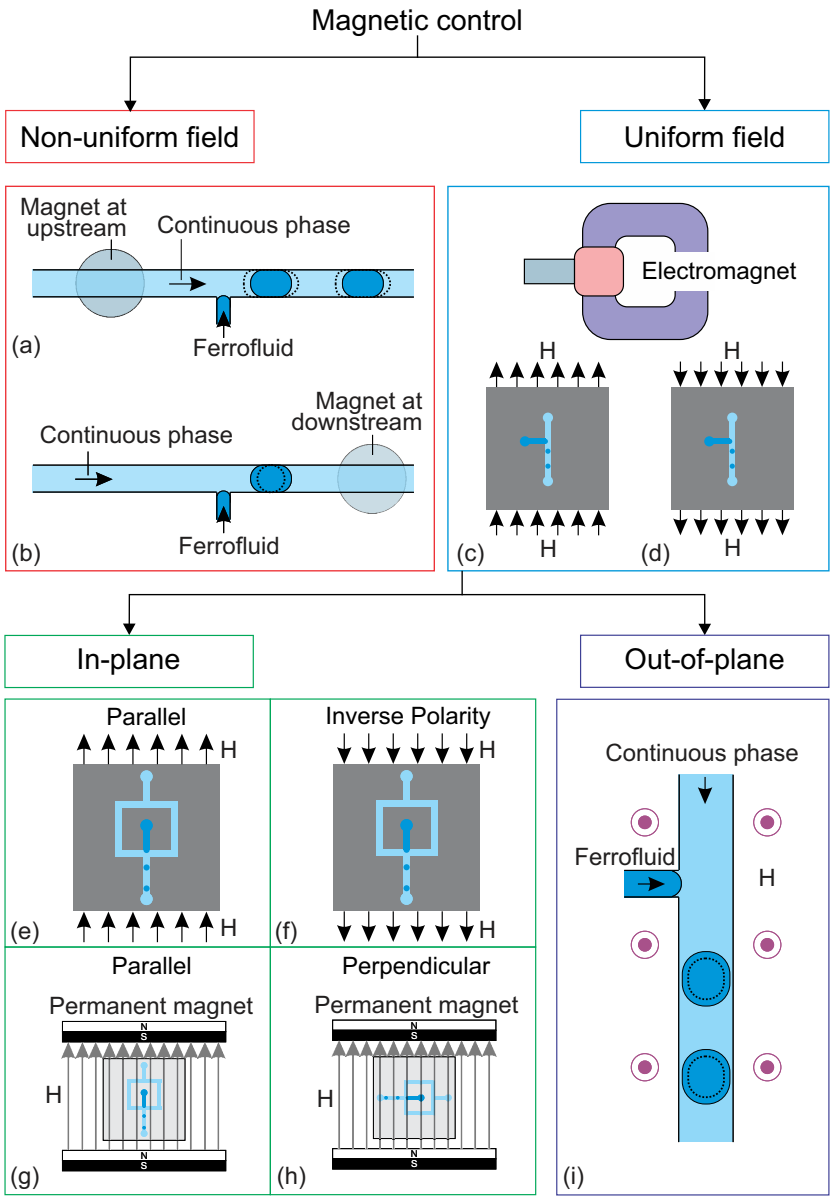

Fig. 4 Classification of the approaches for magnetic control. T-junction device with ferrofluid and magnet[19] at (a) upstream position, (b) at downstream position. Droplet generation in an uniform magnetic field with C-shaped electromagnet,[78,79] (c) direction of the magnetic field, H (d) direction of the magnetic field when the polarity is inversed. Flow focusing junction configuration under homogeneous magnetic field[78] in the direction (e) parallel to the downstream channel (f) inversed polarity from (e). Creation of homogeneous magnetic field using permanent magnets.[80] The in-plane magnetic field could either be (g) parallel to the downstream channel (h) perpendicular to the downstream channel. The gray arrows show the direction of the magnetic field, H. (i) Ferrofluid droplet generation under out-of-plane, homogeneous magnetic field (H).[81] The dotted lines illustrate the changes after activation of the magnetic control.

the surfactant coating. Thus, thermal energy can overcome magnetic potential and evenly distributes the magnetic particles by Brownian motion.[90] Ferrofluid can be treated as a continuum.[89] Ferrofluids are superparamagnetic and can be magnetized without magnetic memory. The nanoparticles in a ferrofluid become non-magnetic once the external magnetic field is removed.[82] A ferrofluid can either be oil-based or water-based. Ferrofluids have been used in microfluidics to manipulate droplet generation magnetically, Fig. 4.

Droplet generation with a water-based ferrofluid was first reported by Nguyen's group.[19] The ferrofluid is injected through a T-junction as the dispersed phase, Fig. 4(a-b). A small circular neodymium iron boron (NdFeB) magnet (3 mm in diameter, 2 mm thick) was placed under the device to influence the generation process. The strength and the direction of the magnetic field were adjusted by the position of the permanent magnet. Under a set of constant flow rates, the droplet size changes when the magnet is placed upstream, Fig. 4(a), or downstream, Fig. 4(b), of the T-junction. The induced magnetic force may delay or accelerate the generation process leading to the different droplet sizes. The magnetic effect decreases with increasing total flow rate due to the larger pressure and viscous

forces.

Magnetic control is applicable to an existing droplet generating device with a slight modification to place the permanent magnet. Since ferrofluid is the dispersed phase, the droplet may not be suitable for samples that are not compatible with the ferrofluid. Furthermore, the magnetic gradient is fixed due to the placement of a relatively large permanent magnet. Thus, the strength of the induced force may not be enough to control the generation process, especially at a high generation frequency. This is why the initial setup[19] was improved in Nguyen's later works with a C-shaped electromagnet,[78,79] Fig. 4(c-d). This setup allows the convenient adjustment of the magnetic field strength by varying the applied current to the electromagnet. Droplet size decreases with increasing magnetic field applied along the main channel of the T-junction, Fig. 4(c). Interestingly, this behavior does not change with the opposite field polarity, Fig. 4(d).[91] The ferrofluid aligns itself with the magnetic field and is stretched along the field direction leading to faster breakup and smaller droplets. This phenomenon is independent of the polarity of the magnetic field, producing similar results for both polarities.

When the same uniform magnetic field is applied to a flow-focusing configuration, droplet size increases with increasing magnetic flux density. The magnetic field is parallel to the main channel, Fig. 4(e). The ferrofluid stream is stretched along the magnetic field direction. Secondary flows are formed within the ferrofluid tip resulting from the alignment of the nanoparticles to the magnetic field.[78] These two factors slow down the breakup process and consequently increase the droplet size. Similar to the T-junction, this effect is independent of the polarity of the magnetic field, Fig. 4(f).

The experimental results obtained from the flow-focusing configuration were consistent with the simulation based on finite volume method and particle level set method. The model utilized the augmented Navier-Stokes equation coupled with interfacial force and magnetic force[79]:

$$\frac{\partial}{\partial t}(\rho\vec{u}) + \nabla\cdot(\rho\vec{u}\vec{u}) = -\nabla p + \nabla\cdot[\eta(\nabla\vec{u}+\nabla\vec{u}^T)] - \gamma\kappa\vec{n}_f D(\phi) - \frac{1}{2}\mu_0|\vec{H}|^2\nabla\chi_m, \quad (7)$$

where the third term on the right side is the interfacial force and the last term is the magnetic force. Consistently with experiments, simulation showed that in the presence of a magnetic field, the tip of the ferrofluid is stretched forward and the formation time is longer, promoting the formation of larger droplets.

Wu et al further investigated the generation process of ferrofluid droplets by applying in-plane, homogeneous magnetic field on a flow-focusing configuration.[80] The results are consistent with previous studies with the applied magnetic field parallel to the downstream channel, Fig. 4(g). Furthermore, the droplet size also increases with the magnetic field perpendicular to the downstream channel, Fig. 4(h). Although both field directions increase the droplet size, the droplet generation mechanisms are different. The emerging droplet is stretched sidewards when the magnetic field is applied perpendicular to the downstream channel. As results, the forming droplet delays the breakup leading to a larger size.

The generation process of a ferrofluid droplet also responds to an out-of-plane, homogeneous magnetic field.[81] Lee et al. investigated the generation of ferrofluid droplets in a T-junction configuration, Fig. 4(i). The generation frequency decreases as the applied field strength increases. At the first observation, the results seem to violate mass conservation as the measured droplet diameter is proportional to the generation frequency. However, a more detailed analysis shows that the results still follow mass conservation. The droplet deforms from a hemisphere to a hemiellipsoid after being exposed to the magnetic field, making the hemiellipsoidal droplet diameter appears smaller as viewed from top, while the droplet volume actually increases. To our best knowledge, magnetic control of droplet generation has been applied only to ferrofluid as the dispersed phase. Magnetic control of droplet generation is still emerging with much room for new discoveries. For instance, the generation of aqueous droplets in an oil-based ferrofluid has not been explored.

5 Mechanical control

Mechanical control of droplet generation involves physical deformation of the liquid interface using hydraulic, pneumatic or piezoelectric actuation. Piezoelectric actuation will be discussed separately from the former two methods as it has an unique characteristics caused by the much faster response time.

5.1 Hydraulic/pneumatic control

Hydraulic and pneumatic actuations are usually executed by valves integrated into the microfluidic devices. Generally, the valves are made of the same elastic device material such as PDMS. The valves are actuated pneumatically using compressed air or hydraulically by applying pressure to the liquid filled valve chamber. If the characteristic time t_v of the actuation has the same order of magnitude of droplet generation time t_d, the actuation is considered as dynamic. The droplet generation is controlled by the transient effect of the valves. In contrast, the actuation is considered static if $t_v \gg t_d$. Fig. 5 summarizes the different approaches of active control with hydraulic and pneumatic actuation.

5.1.1 Perturbation method

The frequency of droplet generation $f = t_d^{-1}$ can be influenced by imposing physical perturbation near the generation site. Willaime et al.[92] created the perturbation with a vibrating mechanical valve integrated at the side channel of the T-junction. The device was fabricated using multilayer soft lithography, Fig. 5(a-b). The top and bottom layers bear the actuation channel and the flow channel, respectively. A PDMS membrane is sandwiched between the two layers and serves as the valve membrane. Water in the valve channels deflects the membrane when a pressure is applied.

At a fixed set of flow rates without perturbation, the T-junction

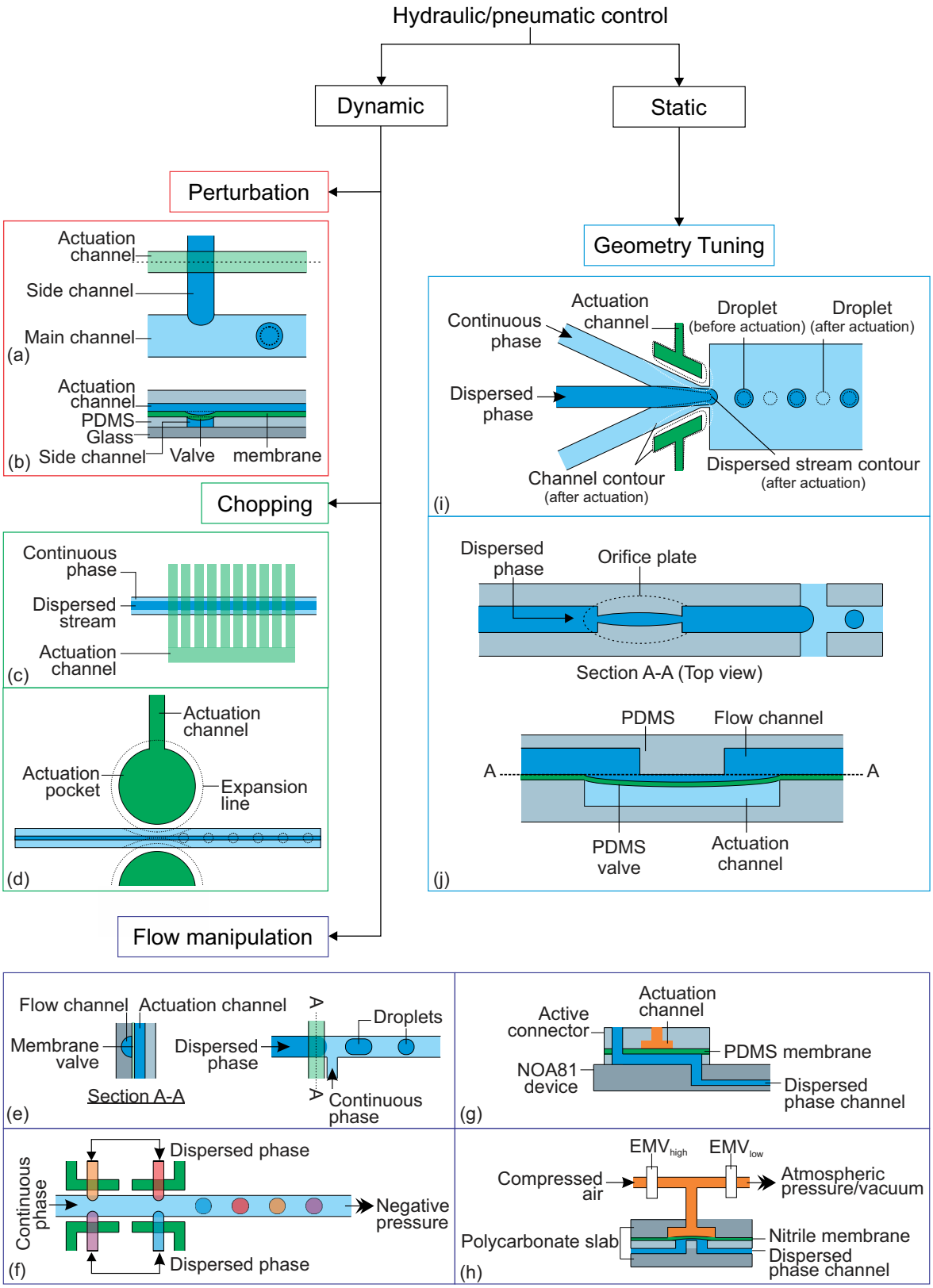

Fig. 5 Classification of the hydraulic/pneumatic control approaches. (a) T-junction with actuation channel[92] (b) Side view along the actuation channel (dashed line); (c) Actuation channels connected to 10 valves which are used to chop the dispersed stream into individual droplets[93] (d) Horizontal moving valve connected to actuation channel;[94] (e) On demand droplet generation using rounded profile T-junction channel and membrane valve;[95] (f) Multiples of T-junctions to produce droplets with distinct composition;[96] (g) Stiff NOA81 device with active connector;[97] (h) Polycarbonate slabs with nitrile membrane;[98] (i) A valve is actuated by expanding the actuation channel pneumatically. This reduces the channel size around the orifice and obstructs the dispersed phase stream, resulting in a reduction of the droplet size;[99] (j) Integrated adjustable orifice plate at the dispersed phase channel. The dotted lines illustrate the changes after activation of the hydraulic/pneumatic control.[100]

Table 4 Magnetic control

Source	Magnetic field	Flow channel geometry[1]	Fluids[2]	Notes
19	non-uniform	T-junction: H = 100 Main W = 300, Side W = 50	C = Silicone oil (100 cSt.s) D = Ferrotech EMG 807	B <28 mT
78,79	Uniform, in-plane, parallel to downstream channel	Flow focusing: H = 100, W = 100 Orifice W = 45	C = Silicone oil (100 cSt.s) D = Ferrotech EMG 807	B <45 mT
91	Uniform, in-plane, parallel to downstream channel	Flow focusing: H = 100, W = 100 Orifice W = 50 T-junction: H = 100 Main W = 150, Side W = 50	C = Silicone oil (100 cSt.s) D = Ferrotech EMG 807	B <45 mT
80	Uniform, in-plane, parallel and perpendicular to downstream channel	Flow focusing: H = 400, W = 400	C = Mineral oil + 4% Span 20 D = Ferrotech EMG 807	B <32 mT
81	Uniform, out-of-plane	T-junction: H = 90 Main W = 80, Side W = 50	C = Tripropylene glycol diacrylate (TPGDA) D = Ferrotech EMG 705	B <9 mT

[1] H - height in μm; W - width in μm [2] C - continuous phase; D - dispersed phase

generates droplets steadily with a fundamental frequency, $f = f_0$. The generation frequency, f, changed after introducing the system perturbation. The droplets could either be generated irregularly with high variation in droplet sizes (quasiperiodic regime), or regularly with f correlated with the perturbation frequency, f_p (synchronized regime). In the synchronized regime, f_p is near to f_0 or a multiples of f_0. For instance, if the pressure amplitude ranges from 0.7 to 1.4 bar, with $Q_d = 18$ and $Q_c = 240\ \mu L\ h^{-1}$, the synchronized regime appears at frequency ratio of:

$$f_p/f_0 \approx 1, \frac{3}{2}, 2, 3, 4, 5, \tag{8}$$

where the generation frequency, f, for each case is synchronized with f_p in the following manner

$$f/f_p = 1, \frac{2}{3}, \frac{1}{2}, \frac{1}{3}, \frac{1}{4}, \frac{1}{5}, \tag{9}$$

respectively.

Choosing a suitable pressure amplitude and plotting the susceptibility ($S = \frac{\partial f_0}{\partial Q_d}$) against f_0/f_p, an optimized flow rate Q_d can be found within a wide range of f_p producing $f/f_p = 1$. Obtaining a wide range of generation frequencies f and droplet sizes at a fixed set of flow rates is important to achieve active control. For instance, with $P = 1.7\ bar$, fixed flow rates of $Q_d = 6$ and $Q_c = 240\ \mu L\ h^{-1}$ the system can deliver a generation frequency f from 2 to 30 Hz at and a corresponding droplet volume from 100 to 1000 pL. The advantage of this design is the small perturbation needed to influence the droplet generation frequency. However, the system needs to be fully characterized to determine the optimized flow rates and pressure amplitude for the synchronized droplet generation. The applicable flow rates are limited as for most of the flow rates, the perturbation induces the quasiperiodic regime that produces droplet with irregular period and size.

5.1.2 Chopping method

Instead of using the vibrating valve to perturb the system, Lee's group incorporated a train of ten similar valves as choppers to cut a prefocused dispersed stream into droplets.[93] The narrow stream was formed by the continuous phase at the cross junction in a stable condition all the way to the outlet. The valves are located near to the outlet of the channel and connected to a common actuation channel, Fig. 5(c). Compared to perturbation method, the chopping method presents a direct way to produce droplet at a desired frequency. This method also allows droplets to be formed at a high flow rate ratio between the dispersed and the continuous phase, because the chopping force from the valves is significantly higher than the viscous force imposed by the continuous phase. However, the generation frequency of this technique is limited by the actuation frequency of the valve. Furthermore, the droplet size disparity could increase as some of the droplets generated upstream could be chopped again by the valves downstream.

Instead of incorporating vertically moving valves that require a multilayer fabrication process, Lee's group later used a pair of horizontally moving valves[94] which were easier to fabricate. The design requires the fabrication of only one layer of PDMS as the actuation channels are now in the same plane as the droplet channel, Fig. 5(d). The horizontally actuating valves deform the main channel, which chops the narrow stream and forms droplets. The drawback of this design is the relatively low generation frequency of only up to 17.4 Hz.

5.1.3 Flow manipulation

When the amplitude of the dynamically actuated valve is large enough to induce intermittent flow on the dispersed phase, droplets can be generated on demand. Lin et al. incorporated a membrane valve on top of a T-junction channel,[95] Fig. 5(e). Droplets are generated at the T-junction by driving the dispersed phase to the main channel and the continuous phase to the side channel with individually controlled pressures. The valve is placed at the main channel, upstream of the junction. The cross section of the flow channel is rounded to facilitate a total blockage of the flow when the valve is closed.

Steady on demand generation of droplet (Steady Drop on Demand, SDOD) was performed by a full control on the instantaneous flow rates, generally of the dispersed phase. Lin et

al.[95] activated the valve periodically while maintaining constant pressures on the dispersed and continuous phases. The resulting droplet volume (V) increases with increasing opening duration (T_0):

$$V = kT_0^a, \tag{10}$$

where k and a are constants that depend on the flow conditions, such as the driving pressures P_d and P_c of the disperse and continuous phases. Since the flow is transient right after opening the valve, it results in $a > 1$. Transient flow occurs as consequence of the abrupt negative pressure gradient created during the retreat of the membrane. The transient effect was found to decrease, yielding $a \approx 1$ with increasing ratio of P_d/P_c. The relationship (eqn 10) is empirical. Hydrodynamic factors such as flow impedance and viscosity of fluids were not considered.

SDOD provides extra degrees of freedom for the controllability of the droplet generation process. The approach is able to produce a selected droplet volume within a large range. Also, the timing of the droplet generation is fully controllable.[95] However, the frequency of the droplet generation is limited by the time taken to open or close the valves. As a result, the frequency of droplet generation is limited to under 20 Hz. The system by Lin et al. requires a round profile to allow sufficient flow blockage when the valve is fully expanded. The channel cannot be fabricated using SU-8 resin unless it is post-processed using photo-polymerization technique.[101]

Woon et al. proposed a predictive model for Drop on Demand (DOD) generation.[102] The dispersed phase was introduced from the side channel and the continuous phase through the central one. Using the analogy to an electronic circuit, a fluidic circuit model was formulated. The flow rate of the dispensed phase (Q_d) was determined by solving the equations with Kirchhoff's circuit laws. Finally, the theoretical droplet volume can be simply calculated as $V_{theo} = Q_d t$, where t is the activation time. Instead of the applied pressure at the inlet, Zeng et al.[96] used negative pressure at the outlet for the DOD concept. The droplet size measured in area increased linearly with T_o in the pressure range from -28.6 to -44.4 kPa. With the pressure as a single driving parameter, the system is easy to operate. Multiple T-junctions with individually controllable pneumatic valves allow for the generation of droplets from different sources, Fig. 5(f).

Ochs et al. design pincer microvalves that do not only allow DOD generation but also the control of dispersed phase flow rate.[103] Leung et al., on the other hand, embedded series of microvalves that makes programmable droplet-based microfluidic device for sample compartmentalization.[104]

The response of DOD can be further improved using devices made of a stiff material.[97] However, integrated membrane valves can only be fabricated in devices made of elastomer such as PDMS. Galas et al. solved this problem by decoupling the device design from the flow controlling system.[97] An active connector made of PDMS with an integrated membrane valve controls the flow of the dispersed phase, Fig. 5(g). The rest of the device is made of a hard material (NOA81).

Churski et al. reported a similar approach using a stiff device and an external valve module.[98,105] The module is modified from an off-the-shelf electromagnetic valve (EMV) to reduce the flow through the valve and lessen the build-up pressure at the downstream.[105] It can also be modified from an EMV using a slab of polycarbonate and a nitrile membrane.[98] In order to shorten further the opening and closing time of valve, a pair of EMVs is also used for each inlet (Fig. 5(h)).[98] EMV_{high} is connected to a compressed air source while EMV_{low} is connected to atmospheric pressure or vacuum. As a result, the minimum time T_0 required for on demand generation is reduced to 25 ms, about half the time needed by a setup using one EMV only. In their later work, Churski et al. also provides practical guidelines for the use of low-cost EMV to generate nanoliter droplets on demand.[34]

5.1.4 Geometry tuning

Lee's group used statically actuated valve for active droplet generation.[106] The horizontally moving valve is located along one side of the downstream channel. The activated valve reduces the width of the channel leading to a narrower stream of pre-focused dispersed phase and consequently smaller droplets. The same valve type was used in a flow-focusing device without the chopping mechanism,[99] Fig. 5(i). The valves allows the size of the orifice to be tuned. Since each valve can be controlled separately, the orifice can be tuned off the center changing the trajectory of the generated droplets downstream.

Abate et al. investigated the control of droplet formation further, using the same type of actuation.[32] The valves are incorporated at the orifice downstream of a flow-focusing junction. The droplet size decreases and the generation frequency increases with decreasing orifice cross section:

$$d_d \sim \frac{\gamma d_0}{\eta_c u_c}, \tag{11}$$

where d_d, γ, d_o, η_c and u_c are droplet diameter, interfacial tension, orifice diameter, continuous phase viscosity and continuous phase velocity, respectively. However, the relationship (11) remains empirical, as it is challenging to predict the cross section of the orifice deformed by the valves. Thus, the droplet size and the applied pressure have to be characterized experimentally.

Statically actuated valves tuning the channel geometry allow the control over a wider range of generation frequencies than the dynamically actuated counterparts. Dynamically actuated valves allow the generation on demand of virtually any polydisperse distribution droplet size with a characteristic time as short as the valve response time. Statically actuated valves cover a wider range of overall frequencies for a fixed monodisperse size. A similar concept was applied to a T-junction device using a horizontally moving valve.[107] The location of the valve is significant for the generation process. A valve located downstream of the junction easily reduces the droplet size. A valve placed the upstream of the junction does not affect the droplet size.

Lee's group also used a statically actuated valve in the disperse phase channel,[100] Fig. 5(j). The channel size is tuned by varying

Table 5 Hydraulic/pneumatic control

Source	Mechanism	Flow channel geometry[1]	Fluids[2]	Notes
92	Perturbation	T-junction: H = 20 or 40 Main W = 200	C=Tetradecane + 1-3% Span 80 D=DI water + fluorescein	Perturbation frequency = 2-13 Hz * Side W is not stated
93,94	Chopping	Flow focusing: H = 100 W = 60	C = Trioctanoin + Polyglyceryl-2 Sesquiisostearate + PEG-10 Polyglyceryl-2 Laurate D = DI water + 0.1% Vitamin C	Chopping frequency: <17 Hz
95	Flow manipulation	T-junction: H = 25 Main & side W = 150	C = Oleic acid/hexadecane/silicone oil + 5% Span 80 D = DI water	Dispensing time >50 ms
102	Flow manipulation	T-junction: H = 11.5, 13.6, 15.3 Main W = 90 Side W = 50	C = Mineral oil D = Water+10% pigment solution/sodium alginate solution (0.1% or 0.5%)	Dispensing time >40 ms
96	Flow manipulation	T-junction: H = 200 Main W = 200 Side W = 240	C = Oleic acid + 2.5% Span 80 D = Water + diluted colored ink	Dispensing time >50 ms
97	Flow manipulation	T-junction: H = 80, Main W = 200	C = Mineral oil + 4.5% Span 80 + 0.4% Tween 80 + 0.05% Triton X100 D = Water+red dye	Dispensing time >40 ms * Side W is not stated
98	Flow manipulation	T-junction: H = 200, Main W = 400	C = Hexadecane + 2% Span 80 D = Water	Dispensing time >25 ms * Side W is not stated
99,106	Geometry tuning	Flow focusing: H = 100 W = 100 Orifice W = 70	C = DI water + 5% Triton X-100 D = Olive oil	Droplet formation frequency <24 Hz
32	Geometry tuning	Flow focusing: H=50 W=20	C = HFE-7500 fluorocarbon + 5% 1H,1H,2H,2H-perfluoro-1-octanol + 1.8% fluorosurfactant ammonium carboxylate D = Water	Droplet formation frequency <3000 Hz
107	Geometry tuning	T-junction: H = 100 Main W = 150 Side W = 100	C = Squalene oil + DDAB + negative-charged DNA modules D = DI water + 2.5% Tween 20	Droplet formation frequency <4000 Hz
100	Geometry tuning	Flow focusing: H = 50 W = 85	C = Olive oil D = DI water + 3% Triton X-100	Droplet formation frequency <96 Hz

[1] H - height in μm; W - width in μm [2] C - continuous phase; D - dispersed phase

the negative actuation pressure. As the pressure in the actuation channel decreases, the channel cross section increases, reducing the velocity of the disperse phase. However, the streamlines become more concentrated at the centerline when the fluid exits the restriction with a higher velocity. In the flow-focusing configuration, the dispersed phase stream appears to be finer and consequently produces smaller droplets. Compared to other tunable designs, this device generates small droplets without deforming the channel excessively.

5.2 Piezoelectricity control

Piezoelectricity is used for a variety of applications such as sound/ultrasound generation, mechanical actuation, sensing and signal processing.[108] Piezoelectric actuation has also been used to control microfluidic droplet generation. The control approaches can be categorized according to the function of the piezoelectric element, Fig. 6. For dispensing purposes, a piezoelectric actuator can be used to supply a fixed amount of dispersed phase for on-demand droplet generation as in ink-jet printing applications. On the other hand, piezoelectric actuation can disturb the interface between continuous and disperse phases and affects the droplet generation process.

5.2.1 Dispensing droplets on demand

Xu et al. used piezoelectric actuation to dispense individual drops.[109] The T-junction device has a chamber filled with the dispersed phase, Fig. 6(a). The top of the chamber consists of a 180 μm-thick PDMS membrane , a 90-μm double-sided adhesive and a piezo bimorph actuator. An actuation pulse induces energy that overcomes the interfacial tension and injects a droplet into the continuous phase:

$$U_s = \pi d^2 \gamma, \tag{12}$$

where d and γ are the diameter of the new droplet and the interfacial tension, respectively. The efficiency of the energy conversion from actuator to surface generation is about 0.9%, given that most of the energy is lost through viscous dissipation.[109] The induced energy is estimated as:

$$W = \frac{3^2}{2 \times 8^2} d_{31}^2 E^2 Y V, \tag{13}$$

where d_{31}, E, Y and V are the strain coefficient, applied electric field, elastic modulus, and volume of the piezo, respectively.

The droplet size is controlled by tuning the duration of the driving pulse and its voltage. Compared to the previously

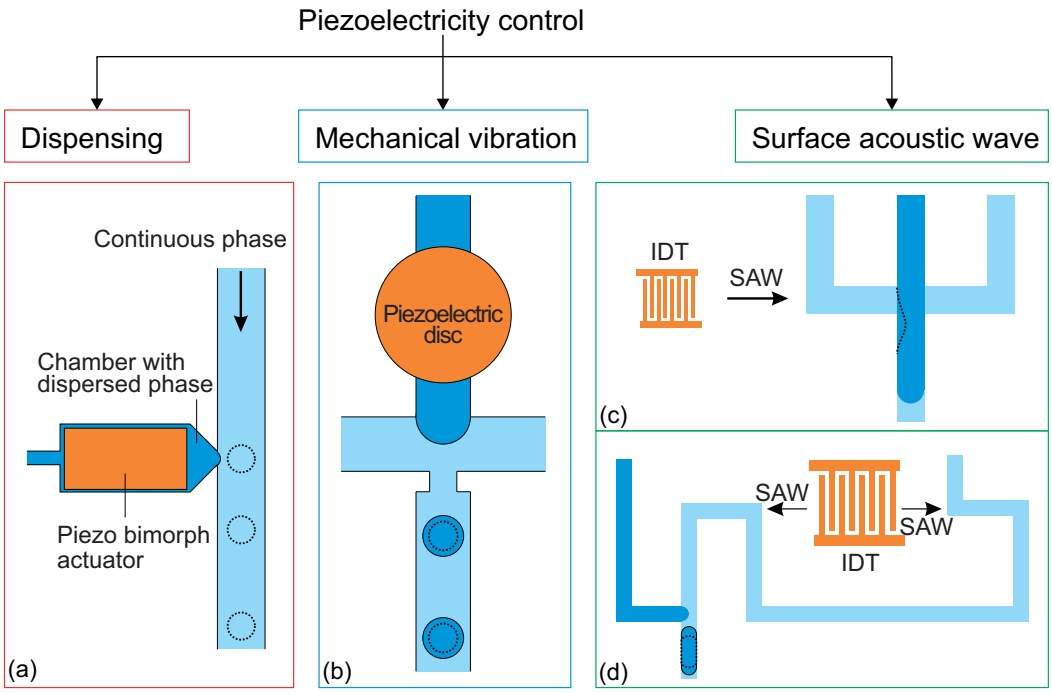

Fig. 6 Classification of the approaches for piezoelectricity control (a) T-junction integrated with piezo bimorph actuator[109] (b) Flow focusing device with piezoelectric disc to vibrate the oil-water interface formed during the droplet generation process[110,111] (c) Flow focusing device integrated with interdigital transducer (IDT) to generate SAW[112] (d) T-junction integrated with IDT without the SAW influencing oil-water interface. The dotted lines illustrate the changes after activation of the piezoelectricity control.[113]

mentioned on-demand droplet generation approaches using pneumatic/hydraulic actuation, piezoelectric actuation is faster. While pneumatic/hydraulic actuation allows for 40-ms dispensing time, piezoelectric actuation can achieve 200 μs. The shorter dispensing time increases the generation frequency by more than two orders of magnitude. In addition to the simple one-by-one droplet dispensing mode, controlling the pulse patterns can generate droplets with different volumes. Dispensing a doublet or the generation of two droplets per pulse were demonstrated. This droplet dispensing approach involves large, rapid movement of the oil-water interface, which may lead to the formation of satellite droplets. Furthermore, the duration of the device is challenged as large chamber deformations are required to produce a droplet. Bransky et al. used piezoelectric dispensing of individual droplets in a flow focusing configuration.[114] Compared to T-junction configuration, the actuation chamber is smaller, as the flow-focusing configuration locally amplifies the pressure on the liquid interface. The smaller chamber also eliminates the generation of satellite droplets due to the smaller deformation at the oil-water interface. The location of the oil-water interfaces adjusted by the height of each liquid.

Apart from attaching piezoelectric actuator on the device for dispensing purpose, Shemesh et al. and Jakiela et al. also attached the actuator externally.[115,116] The working principle is similar to the mechanism of flow manipulation using electromagnetic valves (EMV) discussed in mechanical control section. Though, EMVs has much slower response compared to piezoelectric actuator.[116]

5.2.2 Mechanical vibration

Piezoelectric actuation can be activated periodically to induce mechanical vibration on the oil-water interface. The droplet formation process is affected even if the vibration frequency is only about one order of magnitude higher than the droplet generation frequency. Cheung et al. used this approach to control the droplet generation.[110,111] The vibration is created by a piezoelectric disc attached on top of the dispersed phase channel, Fig. 6(b). Driven by a sinusoidal voltage with an amplitude of 100 to 250 V_{pp}, the piezoelectric disc vibrates with a frequency much higher than that of the droplet generation. The flow rates for both dispersed and continuous phase, were fixed. For the whole set of flow rates tested in that study, the droplet size decreases with the vibration. The droplet size decreases with the increasing applied voltage. Droplet size also decreases with increasing vibration frequency from 250 to 750 Hz. The faster advancement of the oil-water interface to the orifice leads to an earlier breakup of the interface and a smaller droplet size.

Ziemecka et al. uses a similar setup to perturb an originally stable capillary jet formed at the flow focusing junction.[117] As the jet travels downstream, it breaks into droplets with sizes dictated by the imposed perturbation wavelength. Sometimes, the newly formed droplet may further break up into two daughter droplets as it moves downstream. Under a constant flow rate, the droplet size decreases with increasing vibration frequency f_v:

$$q_d = f_v N V, \tag{14}$$

Table 6 Piezoelectric control

Source	Mechanism	Flow channel geometry[1]	Fluids[2]	Notes
[109]	Dispensing	T-junction: H = 50-100, Main W = 250 Nozzle W = 25-100	C = hexadecane D = water	Dispensing frequency <2.5 kHz
[114]	Dispensing	T-junction: H=50 Side W to channel W ratio = $\frac{1}{2}$ and 1 Flow focusing: H=50 Orifice W to channel W ratio = $\frac{1}{2}$ and 1	C = Oleic acid D = DI water	Dispensing frequency <500 Hz
[110]	Mechanical vibration	Flow focusing: H=100, Main W = 150 Orifice W = 40	C = Mineral oil M5904 (light, 32 mPa s), paraffin oil 76235 (116 mPa s), mineral oil 330760 (heavy, 170 mPa s) D = DI water	Vibration frequency = 250 - 750 Hz
[111]	Mechanical vibration	Flow focusing: H = 90, Main W = 150 Orifice W = 40	C = Mineral oil M5904 + 1.2% Span 80 D = DI water	Vibration frequency = 200 - 500 Hz
[117]	Mechanical vibration	Flow focusing: H = 85, W = 100	C = 20% polyethyleneglycol (PEG) in water D = 10% dextran in water	Vibration frequency = 2 - 50 Hz
[118]	Surface acoustic wave	Flow focusing: H=30, W=30	C = HFE-7500 fluorocarbon + 1.8% DuPont Krytox 157 D = Water + bromophenol blue	Actuation frequency = 161 - 171 MHz
[113]	Surface acoustic wave	T-junction: H = 25, Main & side W = 25	C = HFE-7500 fluorocarbon + 1.8% DuPont Krytox 157 D = Water + bromophenol blue	Actuation frequency = 160 MHz
[119]	Surface acoustic wave	T-junction: H = 30, Main W = 30 Side W = 20	C = Olive oil (85 cP) D = Water	Actuation frequency = 48.4 & 95.4 MHz

[1] H - height in μm; W - width in μm [2] C - continuous phase; D - dispersed phase

where q_d, N and V are dispersed phase flow rate, number of droplets in one cycle and droplet volume, respectively. This model yields

$$d = \sqrt[3]{\frac{6q_d}{N\pi f_v}}. \quad (15)$$

5.2.3 Surface acoustic wave (SAW)

In addition to the bulk transmission of vibration used in the approaches described above, surface acoustic wave (SAW) efficiently transfers acoustic energy along the surface of an actuator at its resonance frequency. SAW is excited by an interdigitated transducer (IDT), which is fabricated by patterning a pair of interdigitated comb-like electrodes on a piezoelectric substrate,[112] Fig. 6(c). SAW technology has been used in microfluidics applications such mixing, separation, and droplet sorting.[120]

Schmid et al. used SAW to control the droplet size generated by a flow focusing device under a constant set of flow rates.[118] The PDMS device with the microchannels is bonded directly to a flat piezoelectric $LiNbO_3$ substrate with the IDT, Fig. 6(c). The microchannel was aligned so that the IDT is located on the left side of the junction. The generated SAW travels along the microchannel for the continuous phase. The effect of the SAW on the droplet generation process is obvious upon activating the IDT. The SAW causes an asymmetric excitation of the thinning neck during the break up process, Fig. 6(c). Consequently, the time to breakup is shortened and reduces the droplet size. This phenomenon intensifies with increasing electric power. A stronger SAW shifts the neck and the droplet formation site further downstream with an even shorter break up time. Subsequent study on the control of droplet generation utilized SAW in a T-junction configuration.[113] The IDT is placed far away from the droplet formation site to prevent the SAW from affect the oil-water interface, Fig. 6(d). In this study, the fluids are driven by pressure.

The droplet length decreases with increasing SAW power. The authors hypothesized that the SAW promoted a pressure gradient in the continuous phase. This hypothesis was tested by comparing the pressure at the droplet formation site of the two cases: with and without SAW. The increase in pressure can be related to the volume force generated when SAW couples into the continuous phase.[113] The results of SAW-controlled droplet generation are close to that caused by the pressure increase on the continuous phase.

SAW control is an attractive approach as it allows contactless manipulation. IDT can be located outside of the channel, preventing the electrodes to contact with the fluids directly. Furthermore, IDT allows a small footprint suitable for the integration in a small microfluidic device. However, the fabrication of IDT requires a piezoelectric substrate, whose wetting properties might not be compatible with that of the channel material. Furthermore, a high-performance piezoelectric substrate could be expensive.

Collins et al. integrated a set of focused interdigital transducers (FIDT) on a modified T-junction device to enable on-demand droplet generation using SAW.[119] The curved gold electrodes were patterned with the focal point at the junction. The continuous phase was fed at a constant flow rate by a syringe pump, while the pressure of the dispersed phase was adjusted to form a static oil-water interface at the junction. A

SAW pulse forced the dispersed phase into the main channel. On-demand droplet generation was thus controlled by manipulating the power and the duration of the SAW pulse.

6 Other control methods

6.1 Electrical control with electrorheological fluid

Electrorheological fluids (ERFs) are made of dielectric particles suspended in a carrier fluid.[125] Rheological properties such as viscosity and shear rate changes, if the fluid is subjected to an electric field.[126] Under an electric field, the suspended particles are polarized and aggregate along the field direction.[125] This feature allows the viscosity of the fluid to be electrically controllable, reversibly and continuously, even from the liquid to the solid state. ERFs have already found applications in automotive devices such as engine dampers and vehicle shock absorbers.[126] ERFs have been used in micropumps, microvalves and micromixers.[121] Giant electrorheological fluids (GERFs), a recently developed kind of ERFs with much higher yield strength than the conventional ERFs, were also used in microfluidic devices.[127]

Zhang et al. reported the use of GERF for droplet generation in a microfluidic device.[121] Four fluid contacting electrodes were patterned near the droplet formation junction, Fig. 7(a). The electrodes were made of PDMS-based conducting composites loaded with black carbon nanoparticles. In that setup, GERF was used as the continuous phase while water served as the dispersed phase. Before applying a voltage to the electrodes, long water plugs were formed stably at the junction. This process was interrupted by the application of a voltage on the electrodes stopping the GERF flow. Only water flowed through the junction. If the voltage decreases to a critical value, the GERF rushes again into the junction, breaks the water stream and forms a new droplet. This process allows the generation of droplets to be controlled with the frequency. The same approach was used for a T-junction configuration with similar results. Niu et al. used GERF as the dispersed phase.[122] The carrier fluid of the GERF is sunflower seed oil, which is immiscible with the silicone oil used as the continuous phase. The fabrication of this device is similar to their previous one but the design was changed to suit this approach, Fig. 7(b), only 2 electrodes around the junction were used to control the dispersed phase.

Both control approaches using GERF are attractive as they provide a quick response times of less than 10 ms. The droplet size was determined by the applied frequencies and the shape of the control signal. This feature and control mechanism was adopted to perform 16 logic operations using KCL droplets as the signals.[128] However, given that the fluids are flow-rate driven by syringe pumps, the flow rates of GERF and the other liquid should be carefully selected to prevent bursting of the channels or connections as the pressures build up in each fluid circuit. Another drawback is the concentration of the suspending dielectric particles in the GERF, which is over 20wt% for effective control and might be too high for many applications.

6.2 Photosensitive surfactant

Photosensitive surfactant has been used to make droplet generation controllable by light. Diguet et al. introduced this control method using azobenzene trimethylammonium bromide surfactant (azoTAB).[129] AzoTAB surfactant is available either in trans or cis form under normal room light. Trans(cis) form azoTab converts to cis(trans) form upon illumination of ultra-violet (UV) light.[123] The conversion is reversible, as they restore to their original forms once the UV light is removed. The concept was demonstrated in a flow focusing configuration, where the dispersed phase is water with trans-azoTAB surfactant and the continuous phase is aleic acid. Initially, the flow rates are set to maintain a thin aqueous stream co-flowing with the continuous stream in the center, Fig. 7(c). After exposing the junction to UV light for about 2 s, the middle stream breaks and starts to generate monodisperse droplets, Fig. 7(d). As cis-azoTAB decreases the surface tension of the dispersed stream, the stability of the capillary jet changes to the dripping regime.[16,131] However, the transition does not happen at a high total flow rate, when the system is dominated by viscous forces.[131]

Apart from the jetting/dripping transition, UV light was also used to modify the droplet size under the normal room light. As the UV light is applied and surface tension increases, the droplet breaking site moves upstream, forming larger droplet. With cis-azoTAB (see Fig. 7), the dripping regime (e) turns into jetting regime (f) after being exposed to blue light. This is consistent with the fact that the water stream with trans-azoTAB, which is converted by the blue light from cis-azoTAB, has a lower surface tension than the one with cis-azoTAB. Control with photosensitive surfactant is easy to implement. The system does not require a high concentration azoTAB to have significant effect in control. However, the response for the control is slow as it takes seconds to reach a new stable state after the change of wettability by the respective light.

6.3 Lateral cavity acoustic transducer (LCAT) pump

The pressure rarefaction and compression induced by an acoustic pulse can expand and contract highly compressible bubbles.[132] When bubbles are trapped in the liquid, the application of periodic acoustic pulse vibrates the gas-liquid interface and forms second-order streaming flow in the liquid around the interface.[124,133] This phenomenon of acoustic streaming has been applied for pumping, mixing, sonoporation of suspended cells and sorting of microparticles.[134]

One of the designs using this method is the Lateral Cavity Acoustic Transducer (LCAT), which was introduced by Lee's group in 2008 to pump and mix the fluids.[124] As shown in inset of Fig. 7(g), a LCAT consists of an air pocket formed when fluid passes through the dead-end side channel. The LCAT was activated when a piezoelectric (PZT) disc attached at the bottom of the device is driven by an AC signal. The acoustic wave from PZT vibrates the interface of the air pocket and induces acoustic streaming. That flow provokes a net bulk flow downstream. Integrating multiple LCATs along a channel allows them to collectively work as a pump with a reasonably high driving

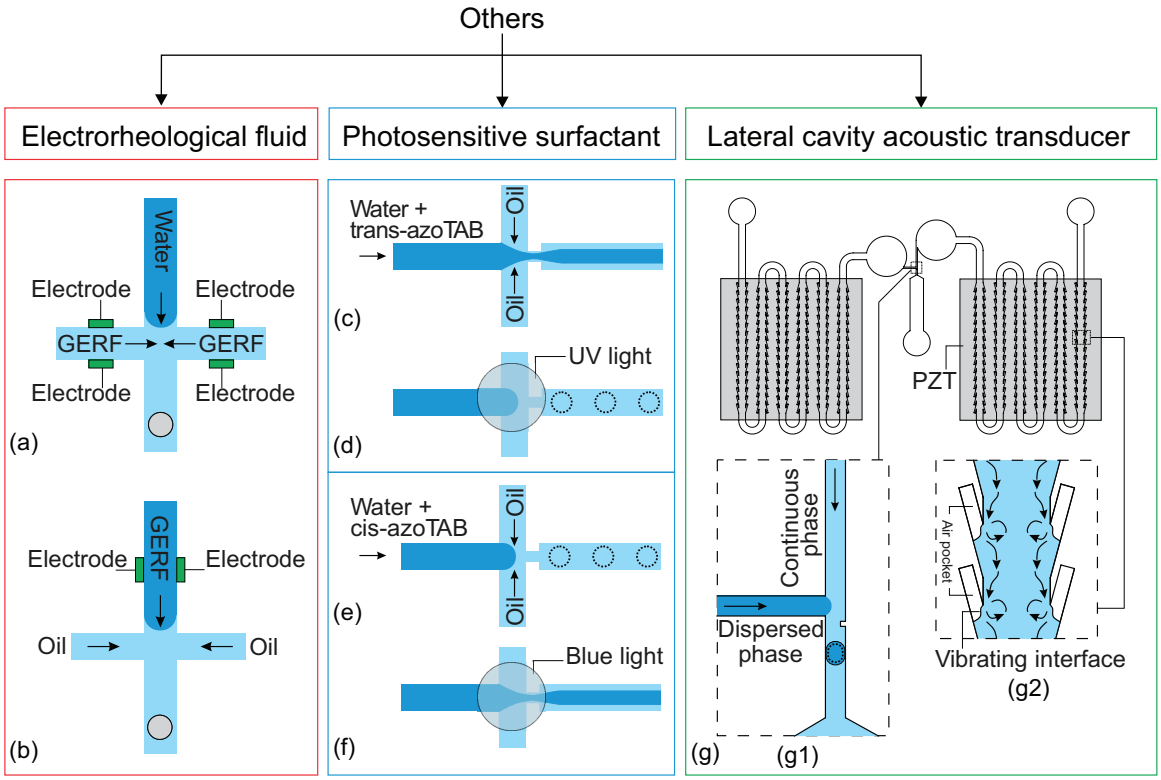

Fig. 7 Flow focusing junction design with electrodes to control the flow rate of (a) continuous phase[121] (b) dispersed phase.[122] (c-d) flow focusing junction with trans-azoTAB photosensitive surfactant in the dispersed phase.[123] (c) before and (d) after activation with UV light. (e-f) with cis-azoTAB in the dispersed phase (e) before activation (f) after activating with blue light. (g) A T-junction droplet generation device integrated with two LCAT pumps:[124] (g1) Droplet generating T-junction with a constriction that facilitates the formation of droplet (g2) Magnified part of the LCATs with the streaming flow generated by the vibrating interface. The dotted lines illustrate the changes after activation of the control.

Table 7 Other control methods

Source	Control method	Flow channel geometry[1]	Fluids[2]	Notes
121	Electrical control with electrorheological fluid	Flow focusing: H = 100, W = 200	C = Sunflower oil based GER fluid D = Water	Voltage < 1.5 kV Frequency < 250 Hz
122	Electrical control with electrorheological fluid	Flow focusing: H = 100, W = 200	C = Silicone oil (50 cSt) D = Sunflower oil based GER fluid	Voltage < 1.5 kV Frequency < 250 Hz
128	Electrical control with electrorheological fluid	Flow focusing: H = 90, W = 200	C = Silicone oil (100 cSt) D = Sunflower oil based GER fluid	Voltage < 450 V
129	Photosensitive surfactant	Flow focusing with orifice: Dispersed phase W = 90 Continuous phase and downstream W = 100 Orifice W = 33	C = Oleic acid D = trans-AzoTAB (12.6 mM) or cis-AzoTAB (14.6 mM) in water	UV illumination at λ = 365 nm * Channel H is not stated
130	Lateral cavity acoustic transducer (LCAT) pump	T-junction: H = 100 Main & side W = 100	W/O droplets C = Mineral oil (20 cp) + 2% Span 80 D = DI water O/W droplets C = DI water + 2% Tween 20 D = Mineral oil (20 cp)	Acoustic frequency = 67.7 kHz Applied Voltage: V_{oil} = 4–9 Vpp V_{water} = 2–6 Vpp

[1] H - height in μm; W - width in μm [2] C - continuous phase; D - dispersed phase

pressure.[135]

LCAT pumps have been integrated in microfluidic droplet generating devices to drive the fluids without using bulky instrument such as a syringe pump and pressure controllers.[130] The device consists of two LCAT pumps, Fig. 7(g). Each pump consisting of 96 pairs of LCATs was activated individually by a PZT to drive one liquid phase. As shown in the inset of Fig. 7(g), droplets are formed at a T-junction. Varying the voltage applied to the PZTs tunes the size of the droplets.

Control of droplet generation using LCAT pumps is attractive as they are small enough to be integrated into a microfluidic device. Compared to the conventional systems, the distance from the pumps to the droplet generating site is reduced significantly. As a result, the flow rates at the generating site can be changed much faster because of the smaller inertia of the system. However, in order to form air pockets of a desirable size and

shape at the LCATs, the channel needs to be both hydrophobic and lipophobic. For this reason, the inner device surface is coated with perfluorodecyltrichlorosilane (FDTS), with limited lifetime of a couple of days. Furthermore, the power of the LCAT pump is still limited, even with the optimized geometry. The maximum generation frequency of the device was 31 Hz, for water in oil droplets and 59.1 Hz oil in water droplets.

7 Conclusions

Microfluidics is one of the enabling technologies in chemical engineering and biotechnology. Controlling the droplet generation process is one of the important and central topics of microfluidics. The control process is physically more complex than processes in other technologies such as microelectronics or photonics. Even with limited geometrical designs and configurations, the various parameters and scales present in the formation of a droplet are far beyond controllability (see for example [136] and references therein). These local degrees of freedom become augmented when rheological properties, hysteretic effects, or issues from biological origin come into play. Further problems such as limited mechanical resistance, reproducibility, or throughput, often early expectations fail when microfluidics technology is translated into practical products.

With this review we aim to provide a comprehensive and systematic overview on active control methods of droplet generation in microfluidics. We summarized different ways for active control of droplet generation. These methods can be classified according to the energy type: (i) electrical, (ii) thermal, (iii) magnetic, (iv) mechanical, and even chemical. In some cases, the control concept involves more than one of those energies. The creativity exhibited by many authors has been admirable. However, reducing the size of the system is becoming the current fundamental challenge for active control.

References

1 P. Gravesen, J. Branebjerg and O. S. Jensen, *Journal of Micromechanics and Microengineering*, 1993, **3**, 168.

2 D. J. Beebe, G. A. Mensing and G. M. Walker, *Annu. Rev. Biomed. Eng.*, 2002, **4**, 261–286.

3 G. M. Whitesides, *Nature*, 2006, **442**, 368–373.

4 D. C. Duffy, J. C. McDonald, O. J. A. Schueller and G. M. Whitesides, *Anal. Chem.*, 1998, **70**, 4974–4984.

5 M. A. Unger, H. P. Chou, T. Thorsen, A. Scherer and S. R. Quake, *Science*, 2000, **288**, 113–116.

6 F. H. A. T. Thorsen, R. W. Roberts and S. R. Quake, *Phys. Rev. Lett.*, 2001, **86**, 4163–4166.

7 S. L. Anna, N. Bontoux and H. A. Stone, *Appl. Phys. Lett.*, 2003, **82**, 364–366.

8 D. B. Bogy, *Annu. Rev. Fluid Mech.*, 1979, **11**, 207–228.

9 J. Eggers, *Rev. Mod. Phys.*, 1997, **69**, 865–929.

10 O. A. Basaran, *AlChE J.*, 2002, **48**, 1842–1848.

11 P. Garstecki, H. A. Stone and G. M. Whitesides, *Phys. Rev. Lett.*, 2005, **94**, 164501.

12 P. Garstecki, M. J. Fuerstman, H. A. Stone and G. M. Whitesides, *Lab. Chip*, 2006, **6**, 437–446.

13 A. Yarin, *Annu. Rev. Fluid Mech.*, 2006, **38**, 159–192.

14 Ö. E. Yildirim and O. A. Basaran, *J. Non-Newtonian Fluid Mech.*, 2006, **136**, 17–37.

15 J. Eggers and E. Villermaux, *Rep. Prog. Phys.*, 2008, **71**, 036601.

16 M. A. Herrada, A. M. Gañán-Calvo and P. Guillot, *Phys. Rev. E*, 2008, **78**, 046312.

17 Z. Nie, M. Seo, S. Xu, P. Lewis, M. Mok, E. Kumacheva, G. Whitesides, P. Garstecki and H. Stone, *Microfluidics and Nanofluidics*, 2008, **5**, 585–594.

18 M. A. Herrada, J. M. Montanero, C. Ferrera and A. M. Gañán-Calvo, *J. Fluid Mech.*, 2010, **649**, 523–536.

19 S. H. Tan, N.-T. Nguyen, L. Yobas and T. Kang, *J. Micromech. Microeng.*, 2010, **20**, 045004.

20 A. M. Gañán-Calvo, *Phys. Rev. Lett.*, 1998, **80**, 285–288.

21 P. Garstecki, I. Gitlin, W. DiLuzio, G. M. Whitesides, E. Kumacheva and H. A. Stone, *Appl. Phys. Lett.*, 2004, **85**, 2649–2651.

22 S. Takeuchi, P. Garstecki, D. B. Weibel and G. M. Whitesides, *Adv. Mater.*, 2005, **17**, 1067–1072.

23 A. M. Gañán-Calvo, R. González-Prieto, P. Riesco-Chueca, M. A. Herrada and M. Flores-Mosquera, *Nature Phys.*, 2007, **3**, 737–742.

24 M. A. Herrada, A. M. Gañán-Calvo, A. Ojeda-Monge, B. Bluth and P. Riesco-Chueca, *Phys. Rev. E*, 2008, **78**, 036323.

25 S. H. Tan, B. Semin and J.-C. Baret, *Lab. Chip*, 2014, **14**, 1099–1106.

26 H. Yu, Z. Z. Chong, S. B. Tor, E. Liu and N. H. Loh, *RSC Adv.*, 2015, **5**, 8377–8388.

27 M. A. Herrada and A. M. Gañán-Calvo, *Phys. Fluids*, 2009, **21**, 042003.

28 A. S. Utada, E. Lorenceau, D. R. Link, P. D. Kaplan, H. A. Stone and D. A. Weitz, *Science*, 2005, **308**, 537–541.

29 A. M. Gañán-Calvo and J. M. Gordillo, *Phys. Rev. Lett.*, 2001, **87**, 274501.

30 A. Gañán-Calvo, *U.S. Patent*, 1998, US 6,116,516.

31 T. Ward, M. Faivre, M. Abkarian and H. A. Stone, *Electrophoresis*, 2005, **26**, 3716–3724.

32 A. R. Abate, M. B. Romanowsky, J. J. Agresti and D. a. Weitz, *Appl. Phys. Lett.*, 2009, **94**, 023503.

33 H. A. Stone, A. D. Stroock and A. Ajdari, *Annu. Rev. Fluid Mech.*, 2004, **36**, 381–411.

34 K. Churski, M. Nowacki, P. M. Korczyk and P. Garstecki, *Lab on a Chip*, 2013, **13**, 3689.

35 R. Seemann, M. Brinkmann and T. P. S. Herminghaus, *Rep. Prog. Phys.*, 2012, **75**, 016601.

36 G. F. Christopher and S. L. Anna, *J. Phys. D. Appl. Phys.*, 2007, **40**, R319–R336.

37 S.-Y. Teh, R. Lin, L.-H. Hung and A. P. Lee, *Lab. Chip*, 2008, **8**, 198–220.

38 C. N. Baroud, F. Gallaire and R. Dangla, *Lab. Chip*, 2010, **10**, 2032–2045.

39 A. B. Theberge, F. Courtois, Y. Schaerli, M. Fischlechner,

C. Abell, F. Hollfelder and W. T. S. Huck, *Angew. Chem. Int. Ed. Engl.*, 2010, **34**, 5846–5868.
40 J.-S. Chen and J.-H. Jiang, *Chinese Journal of Analytical Chemistry*, 2012, **40**, 1293–1300.
41 K.-Y. Song and W.-J. Zhang, *Recent Patents on Nanotechnology*, 2013, **7**, 133–152.
42 C. X. Zhao, *Adv. Drug Deliv. Rev.*, 2013, **65**, 1420–1446.
43 N.-T. Nguyen and S. H. Tan, *Microdroplet Technology*, Springer New York, 2012, pp. 51–75.
44 D. R. Link, E. Grasland-Mongrain, A. Duri, F. Sarrazin, Z. Cheng, G. Cristobal, M. Marquez and D. A. Weitz, *Angew. Chem. Int. Ed.*, 2006, **45**, 2556–2560.
45 H. Kim, D. Luo, D. Link, D. A. Weitz, M. Marquez and Z. Cheng, *Appl. Phys. Lett.*, 2007, **91**, 133106.
46 F. Malloggi, S. A. Vanapalli, H. Gu, D. van den Ende and F. Mugele, *J. Phys.: Condens. Matter*, 2007, **19**, 462101.
47 H. Gu, M. H. G. Duits and F. Mugele, *Lab. Chip*, 2010, **10**, 1550.
48 E. Castro-Hernández, P. García-Sánchez, S. H. Tan, A. M. Gañán-Calvo, J.-C. Baret and A. Ramos, *Microfluidics and Nanofluidics*, 2015, 1–8.
49 C. Ganan and S. Lopez-Herrera, *Dispositif pour la production de jets capillaires et de particules micrometriques et nanometriques*, 2003, WO Patent App. PCT/ES2003/000,065.
50 A. M. Gañán-Calvo, J. M. López-Herrera and P. Riesco-Chueca, *J. Fluid Mech.*, 2006, **566**, 421–445.
51 J. Rodríguez-Rodríguez, A. Sevilla, C. Martínez-Bazán and J. M. Gordillo, *Annu. Rev. Fluid Mech.*, 2015, **47**, 405–429.
52 A. M. Gañán-Calvo, *Phys. Rev. Lett.*, 2007, **98**, 134503.
53 S. H. Tan, N.-T. Nguyen, Y. C. Chua and T. G. Kang, *Biomicrofluidics*, 2010, **4**, 032204.
54 D. A. Saville, *Annu. Rev. Fluid Mech.*, 1997, **29**, 27–64.
55 A. M. Gañán-Calvo, N. Rebollo-Muñoz and J. M. Montanero, *New J. Phys.*, 2013, **15**, 033035.
56 E. Cummings and B. Khusid, *Microfluidic Technologies for Miniaturized Analysis Systems*, Springer US, 2007, pp. 315–355.
57 R. Cody, *Applied Electrospray Mass Spectrometry*, CRC Press, 2002.
58 P. He, H. Kim, D. Luo, M. Marquez and Z. Cheng, *Appl. Phys. Lett.*, 2010, **96**, 174103.
59 F. Mugele and J.-C. Baret, *J. Phys.: Condens. Matter*, 2005, **17**, R705–R774.
60 C. Quilliet and B. Berge, *Current Opinion in Colloid & Interface Science*, 2001, **6**, 34–39.
61 F. Li and F. Mugele, *Appl. Phys. Lett.*, 2008, **92**, 244108.
62 F. Malloggi, H. Gu, A. G. Banpurkar, S. A. Vanapalli and F. Mugele, *Eur. Phys. J. E*, 2008, **26**, 91–96.
63 H. Gu, C. U. Murade, M. H. G. Duits and F. Mugele, *Biomicrofluidics*, 2011, **5**, 011101.
64 H. Gu, F. Malloggi, S. A. Vanapalli and F. Mugele, *Appl. Phys. Lett.*, 2008, **93**, 183507.
65 S. L. Anna and H. C. Mayer, *Phys. Fluids*, 2006, **18**, 121512.
66 T. B. Jones, K.-L. Wang and D.-J. Yao, *Langmuir*, 2004, **20**, 2813–2818.
67 A. C. Siegel, S. S. Shevkoplyas, D. B. Weibel, D. A. Bruzewicz, A. W. Martinez and G. M. Whitesides, *Angew. Chem. Int. Ed.*, 2006, **45**, 6877–6882.
68 S. H. Tan, F. Maes, B. Semin, J. Vrignon and J.-C. Baret, *Scientific Reports*, 2014, **4**, 4787.
69 N.-T. Nguyen, T.-H. Ting, Y.-F. Yap, T.-N. Wong, J. C.-K. Chai, W.-L. Ong, J. Zhou, S. H. Tan and L. Yobas, *Appl. Phys. Lett.*, 2007, **91**, 084102.
70 C. A. Stan, S. K. Y. Tang and G. M. Whitesides, *Anal. Chem.*, 2009, **81**, 2399–2402.
71 C. N. Baroud, J.-P. Delville, F. m. c. Gallaire and R. Wunenburger, *Phys. Rev. E*, 2007, **75**, 046302.
72 S.-Y. Park, T.-H. Wu, Y. Chen, M. A. Teitell and P.-Y. Chiou, *Lab. Chip*, 2011, **11**, 1010.
73 Y.-F. Yap, S. H. Tan, N.-T. Nguyen, S. M. S. Murshed, T.-N. Wong and L. Yobas, *J. Phys. D: Appl. Phys.*, 2009, **42**, 065503.
74 S. M. S. Murshed, S. H. Tan and N.-T. Nguyen, *J. Phys. D: Appl. Phys.*, 2008, **41**, 085502.
75 S. M. S. Murshed, S. H. Tan, N. T. Nguyen, T. N. Wong and L. Yobas, *Microfluidics and Nanofluidics*, 2008, **6**, 253–259.
76 S. H. Tan, S. M. S. Murshed, N.-T. Nguyen, T. N. Wong and L. Yobas, *J. Phys. D: Appl. Phys.*, 2008, **41**, 165501.
77 C. N. Baroud, M. R. de Saint Vincent and J.-P. Delville, *Lab. Chip*, 2007, **7**, 1029.
78 J. Liu, S. H. Tan, Y. F. Yap, M. Y. Ng and N.-T. Nguyen, *Microfluidics and Nanofluidics*, 2011, **11**, 177–187.
79 J. Liu, Y. F. Yap and N.-T. Nguyen, *Phys. Fluids*, 2011, **23**, 072008.
80 Y. Wu, T. Fu, Y. Ma and H. Z. Li, *Soft Matter*, 2013, **9**, 9792.
81 C.-P. Lee, T.-S. Lan and M.-F. Lai, *J. Appl. Phys.*, 2014, **115**, 17B527.
82 N. Pamme, *Lab. Chip*, 2006, **6**, 24–38.
83 Z. Z. Chong, W. J. Sim, Z. T. Yeo, K. H. Li, S. H. Ng, H. Xia, T. N. Wong, N. H. Loh, S. B. Tor, S. H. Tan and N.-T. Nguyen, *Micro and Nanosystems*, 2014, **6**, 232–236.
84 K. Zhang, Q. Liang, X. Ai, P. Hu, Y. Wang and G. Luo, *Lab. Chip*, 2011, **11**, 1271.
85 C.-H. Chen, A. R. Abate, D. Lee, E. M. Terentjev and D. A. Weitz, *Adv. Mater.*, 2009, **21**, 3201–3204.
86 Y. Wu, T. Fu, Y. Ma and H. Z. Li, *Microfluidics and Nanofluidics*, 2014, **18**, 19–27.
87 E. Surenjav, C. Priest, S. Herminghaus and R. Seemann, *Lab. Chip*, 2009, **9**, 325–330.
88 C. P. Lee, H. Y. Tsai and M. F. Lai, *Soft Matter*, 2012, **8**, 11537.
89 N.-T. Nguyen, *Microfluidics and Nanofluidics*, 2011, **12**, 1–16.
90 É. du Trémolet de Lacheisserie, D. Gignoux and M. Schlenker, *Magnetism*, Springer US, 2002, pp. 213–234.

91 S. H. Tan and N.-T. Nguyen, *Phys. Rev. E*, 2011, **84**, 036317.
92 H. Willaime, V. Barbier, L. Kloul, S. Maine and P. Tabeling, *Phys. Rev. Lett.*, 2006, **96**, 054501.
93 C.-T. Chen and G.-B. Lee, *J. Microelectromech. Syst.*, 2006, **15**, 1492–1498.
94 S.-K. Hsiung, C.-T. Chen and G.-B. Lee, *J. Micromechanics Microengineering*, 2006, **16**, 2403–2410.
95 B.-C. Lin and Y.-C. Su, *Journal of Micromechanics and Microengineering*, 2008, **18**, 115005.
96 S. Zeng, B. Li, X. Su, J. Qin and B. Lin, *Lab. Chip*, 2009, **9**, 1340.
97 J.-C. Galas, D. Bartolo and V. Studer, *New J. Phys.*, 2009, **11**, 075027.
98 K. Churski, J. Michalski and P. Garstecki, *Lab. Chip*, 2010, **10**, 512–518.
99 C.-Y. Lee, Y.-H. Lin and G.-B. Lee, *Microfluidics and Nanofluidics*, 2008, **6**, 599–610.
100 J.-H. Wang and G.-B. Lee, *Micromachines*, 2013, **4**, 306–320.
101 W. Park, S. Han and S. Kwon, *Lab. Chip*, 2010, **10**, 2814.
102 W. S. Lee, S. Jambovane, D. Kim and J. W. Hong, *Microfluidics and Nanofluidics*, 2009, **7**, 431–438.
103 C. J. Ochs and A. R. Abate, *Lab Chip*, 2015, **15**, 52–56.
104 K. Leung, H. Zahn, T. Leaver, K. M. Konwar, N. W. Hanson, A. P. Page, C.-C. Lo, P. S. Chain, S. J. Hallam and C. L. Hansen, *Proceedings of the National Academy of Sciences*, 2012, **109**, 7665–7670.
105 K. Churski, P. Korczyk and P. Garstecki, *Lab on a Chip*, 2010, **10**, 816.
106 C.-H. Lee, S.-K. Hsiung and G.-B. Lee, *Journal of Micromechanics and Microengineering*, 2007, **17**, 1121–1129.
107 H.-W. Wu, Y.-C. Huang, C.-L. Wu and G.-B. Lee, *Microfluidics and Nanofluidics*, 2008, **7**, 45–56.
108 W. Heywang, *Piezoelectricity evolution and future of a technology*, Springer, Berlin, 2008.
109 J. Xu and D. Attinger, *Journal of Micromechanics and Microengineering*, 2008, **18**, 065020.
110 Y. N. Cheung and H. Qiu, *Phys. Rev. E*, 2011, **84**, 066310.
111 Y. N. Cheung and H. Qiu, *Journal of Micromechanics and Microengineering*, 2012, **22**, 125003.
112 T. Franke, A. R. Abate, D. A. Weitz and A. Wixforth, *Lab. Chip*, 2009, **9**, 2625.
113 L. Schmid and T. Franke, *Appl. Phys. Lett.*, 2014, **104**, 133501.
114 A. Bransky, N. Korin, M. Khoury and S. Levenberg, *Lab. Chip*, 2009, **9**, 516–520.
115 J. Shemesh, A. Nir, A. Bransky and S. Levenberg, *Lab on a Chip*, 2011, **11**, 3225.
116 S. Jakiela, P. Debski, B. Dabrowski and P. Garstecki, *Micromachines*, 2014, **5**, 1002–1011.
117 I. Ziemecka, V. van Steijn, G. J. M. Koper, M. Rosso, A. M. Brizard, J. H. van Esch and M. T. Kreutzer, *Lab. Chip*, 2011, **11**, 620–624.
118 L. Schmid and T. Franke, *Lab. Chip*, 2013, **13**, 1691–1694.
119 D. J. Collins, T. Alan, K. Helmerson and A. Neild, *Lab. Chip*, 2013, **13**, 3225–3231.
120 X. Ding, P. Li, S.-C. S. Lin, Z. S. Stratton, N. Nama, F. Guo, D. Slotcavage, X. Mao, J. Shi, F. Costanzo and T. J. Huang, *Lab. Chip*, 2013, **13**, 3626.
121 M. Zhang, J. Wu, X. Niu, W. Wen and P. Sheng, *Phys. Rev. E*, 2008, **78**, 066305.
122 X. Niu, M. Zhang, J. Wu, W. Wen and P. Sheng, *Soft Matter*, 2009, **5**, 576–581.
123 C. T. Lee, K. A. Smith and T. A. Hatton, *Macromolecules*, 2004, **37**, 5397–5405.
124 A. R. Tovar and A. P. Lee, *Lab. Chip*, 2009, **9**, 41–43.
125 M. Zhang, X. Gong and W. Wen, *Electrophoresis*, 2009, **30**, 3116–3123.
126 T. Hao, *Electrorheological fluids the non-aqueous suspensions*, Elsevier, Amsterdam Boston, 2005.
127 W. Wen, X. Huang, S. Yang, K. Lu and P. Sheng, *Nat. Mater.*, 2003, **2**, 727–730.
128 M. Zhang, L. Wang, X. Wang, J. Wu, J. Li, X. Gong, J. Qin, W. Li and W. Wen, *Soft Matter*, 2011, **7**, 7493.
129 A. Diguet, H. Li, N. Queyriaux, Y. Chen and D. Baigl, *Lab. Chip*, 2011, **11**, 2666.
130 W.-F. Fang and A. P. Lee, *Microfluidics and Nanofluidics*, 2015, **18**, 1265–1275.
131 A. M. Gañán-Calvo, *Phys. Rev. E*, 2008, **78**, 026304.
132 K. Ferrara, R. Pollard and M. Borden, *Annu. Rev. Biomed. Eng.*, 2007, **9**, 415–447.
133 Z. Z. Chong, S. B. Tor, N. H. Loh, T. N. Wong, A. M. Gañán-Calvo, S. H. Tan and N.-T. Nguyen, *Lab. Chip*, 2015, **15**, 996–999.
134 A. Hashmi, G. Yu, M. Reilly-Collette, G. Heiman and J. Xu, *Lab. Chip*, 2012, **12**, 4216–4227.
135 A. R. Tovar, M. V. Patel and A. P. Lee, *Microfluidics and Nanofluidics*, 2011, **10**, 1269–1278.
136 J. R.Castrejón-Pita, A. A. Castrejón-Pita, S. S. Thete, K. Sambath, I. M. Hutchings, J. Hinch, J. R. Lister and O. A. Basaran, *Proc Natl Acad Sci USA*, 2015, **112**, 4582–4587.